ORIGINAL RESEARCH ARTICLE

Clin Pharmacokinet 2006; 45 (5): 511-542
0312-5963/06/0005-0511/$39.95/0

A Novel Strategy for Physiologically Based Predictions of Human Pharmacokinetics

Hannah M. Jones,[1] *Neil Parrott*,[1] *Karin Jorga*[2] and *Thierry Lavé*[1]

1 Drug Metabolism and Pharmacokinetics, F. Hoffmann-La Roche Ltd, Basel, Switzerland
2 Clinical Pharmacology, F. Hoffmann-La Roche Ltd, Basel, Switzerland

Abstract

Background: The major aim of this study was to develop a strategy for predicting human pharmacokinetics using physiologically based pharmacokinetic (PBPK) modelling. This was compared with allometry (of plasma concentration-time profiles using the Dedrick approach), in order to determine the best approaches and strategies for the prediction of human pharmacokinetics.

Methods: PBPK and Dedrick predictions were made for 19 F. Hoffmann-La Roche compounds. A strategy for the prediction of human pharmacokinetics using PBPK modelling was proposed in this study. Predicted values (pharmacokinetic parameters, plasma concentrations) were compared with observed values obtained after intravenous and oral administration in order to assess the accuracy of the prediction methods.

Results: By following the proposed strategy for PBPK, a prediction would have been made prospectively for approximately 70% of the compounds. The prediction accuracy for these compounds in terms of the percentage of compounds with an average-fold error of <2-fold was 83%, 50%, 75%, 67%, 92% and 100% for apparent oral clearance (CL/F), apparent volume of distribution during terminal phase after oral administration (V_z/F), terminal elimination half-life ($t_{1/2}$), peak plasma concentration (C_{max}), area under the plasma concentration-time curve (AUC) and time to reach C_{max} (t_{max}), respectively. For the other 30% compounds, unacceptable prediction accuracy was obtained in animals; therefore, a prospective prediction of human pharmacokinetics would not have been made using PBPK. For these compounds, prediction accuracy was also poor using the Dedrick approach. In the majority of cases, PBPK gave more accurate predictions of pharmacokinetic parameters and plasma concentration-time profiles than the Dedrick approach.

Conclusions: Based on the dataset evaluated in this study, PBPK gave reasonable predictions of human pharmacokinetics using preclinical data and is the recommended approach in the majority of cases. In addition, PBPK modelling is a useful tool to gain insights into the properties of a compound. Thus, PBPK can guide experimental efforts to obtain the relevant information necessary to understand the compound's properties before entry into human, ultimately resulting in a higher level of prediction accuracy.

Background

During the drug discovery and development process, potential clinical candidates are screened for their absorption, distribution, metabolism and excretion (ADME) properties. In order to avoid failures in the clinic related to poor ADME properties there has been an increased demand to predict human pharmacokinetics as early as possible, thus helping to select the best candidates for development and rejecting those with a low probability of success. Predicting human pharmacokinetics can also assist in (i) choosing the first dose for a clinical trial; (ii) testing the suitability of the compound for the intended dosage regimen; (iii) predicting any interactions; and (iv) predicting the expected variability in humans. Furthermore, predicting human pharmacokinetics prior to phase I studies has been shown to result in significant time savings ranging from 1 to 6 months.[1] Although a large number of methodologies have been established for this purpose, including allometric scaling[2,3] and physiologically based pharmacokinetic (PBPK) modelling,[4,5] there is still no systematic approach to prediction, with many different companies and academic institutions using different approaches.

Allometric scaling of *in vivo* preclinical data has been the traditional approach used for the prediction of human pharmacokinetics. Such techniques have been described in detail in the literature.[2,6,7] These methods assume that any differences across species are determined by body size alone. In this context the main pharmacokinetics parameters (clearance [CL] and volume of distribution at steady state [V_{ss}]), as well as plasma concentration-time profiles (with Dedrick plots), are scaled across species as a power function of bodyweight. Although in some cases these methods give good predictions,[8-10] their physiological basis is questionable and inaccurate results are frequently obtained, particularly when there are large interspecies differences in pharmacokinetic properties.[11,12] For example, this approach does not allow for species' differences in metabolic CL (except those due to differences in bodyweight), therefore reducing its predictive utility when scaling this parameter across species. Attempts have been made to improve predictions in these cases by applying corrections for protein binding, brain weight, maximum life span potential or *in vitro* hepatocyte intrinsic CL (CL_{int}), with some degree of success.[3,9,13,14]

Until recently, the use of PBPK models has been limited in drug discovery and development as a result of the mathematical complexity of the models and the labour intensive input data required; however, advances in the prediction of hepatic metabolism[15,16] and tissue distribution,[17-19] from *in vitro* and *in silico* data, have made these models more attractive. Methodologies available for predicting hepatic metabolism from *in vitro* systems (e.g. hepatocytes and microsomes) have been described in detail by Houston[15] and have been validated extensively in the rat.[20-22] With advances in the storage and availability of human tissue, these approaches have been used successfully to predict human hepatic CL (CL_H) in a number of cases.[16,23,24] Mechanistic equations have been developed by Poulin and coworkers[17-19] for the prediction of *in vivo* tissue **:** plasma partition coefficients (K_ps) and hence distribution in rat, rabbit and human. These equations have greatly extended the applicability of the PBPK approach to early compound research and development by reducing the need for lengthy *in vivo* experiments. Overall, PBPK models provide the opportunity to integrate key input parameters from different sources to not only estimate pharmacokinetic parameters and predict plasma and tissue concentration-time profiles, but also to gain mechanistic insight into the properties of a compound. Although this approach shows much promise, it has not been extensively validated, with only a few reports of its application in the literature,[5,25] mainly for marketed compounds.

The purpose of this work was to propose and evaluate a PBPK strategy for the prediction of human pharmacokinetics. Secondly, its predictive ability was compared retrospectively with allometry (of plasma concentration-time profiles using the Dedrick approach) for a series of F. Hoffmann-La Roche compounds that reached clinical development between 1998 and 2002. The compounds se-

lected covered a wide range of physicochemical properties and therapeutic areas. The ultimate aim was to determine the best approaches and strategies for the prediction of human pharmacokinetics and to make some recommendation on the input data required for more reliable predictions.

Methods

Compound Selection

The original set of compounds included in this analysis represented all the compounds developed at F. Hoffmann-La Roche that went into clinical development between 1998 and 2002. From this set, biological compounds, prodrugs and compounds that were not intended to be absorbed were excluded. The remaining compounds (n = 19) were used in this analysis. Clinical data were available for these compounds at a range of doses after intravenous infusion (infusion time 0.073–0.50 hours) or oral administration. Summaries of the available *in vitro*, physicochemical and pharmacokinetic data for all 19 compounds are shown in table I, table II and table III. The compounds selected cover a wide range of physicochemical and pharmacokinetic properties. All compounds were lipophilic, with LogP values ranging between 1.2 and 6.6, with a mean of 4. Five compounds were acids with a dissociation constant (pKa) <8, seven were bases with a pKa >6 and seven were neutral or weakly ionised at physiological pH. Terminal elimination half-life ($t_{1/2}$) in humans ranged from short (0.50 hours) to long (>200 hours). Elimination pathways included hepatic metabolism, renal excretion, biliary excretion or a combination of these. Plasma protein binding values ranged from extensive to low (fraction unbound in plasma [f_{up}] from 0.00060 to 0.90). Distribution characteristics consisted of both passive and active processes and varied from limited to widespread. In the rat, the percentage absorbed ranged from 15% to 100%.

Physiologically Based Pharmacokinetic (PBPK) Approach

Model Structure

The generic PBPK model used in this study was composed of 15 compartments, namely adipose tissue, bone, brain, gut, heart, kidney, liver, lung, muscle, rest of body, skin, spleen and testes, which were linked together by the blood circulation (arterial and venous). Perfusion rate-limited kinetics was assumed; each tissue was represented by a single well-stirred compartment, limited by blood flow. This assumes that the drug distributes instantaneously into the whole tissue from the incoming blood flow and that there are no concentration gradients within the tissue. The liver and kidney were considered the only sites of elimination. The mathematical model was written in the simulation software ModelMaker, version 3.0.4 (Cherwell Scientific Ltd, Oxford Science Park, Oxford, UK). The following mass balance differential equations were used in the model.

For non-eliminating tissues (adipose, bone, brain, heart, muscle, skin, spleen and testes) [equation 1]:

$$V_T \bullet dC_T / dt = Q_T \bullet C_{ab} - Q_T \bullet C_{vT} \quad \text{(Eq. 1)}$$

where Q is blood flow (L/h), C is concentration (mg/L), V is volume (L), T is tissues, ab is arterial blood, venous (v) tissue concentration (C_{vT}) is $C_T/(K_{pT}/b : p)$, b : p is blood to plasma ratio, and t is time.

For liver (equation 2):

$$V_{LI} \bullet dC_{LI} / dt = Q_H \bullet C_{ab} + Q_{GU} \bullet C_{vGU} + Q_{SL} \bullet C_{vSL} - Q_{LI} \bullet C_{vLI} - \textit{in vivo}\ CL_{int,u} \bullet C_{vLI,u} \quad \text{(Eq. 2)}$$

where LI is liver, H is hepatic, GU is gut, SL is spleen; $Q_{LI} = Q_H + Q_{GU} + Q_{SL}$, $C_{vLI,u}$ is unbound venous liver concentration, $CL_{int,u}$ is scaled, unbound *in vivo* CL_{int} (L/h).

For kidney (equation 3):

$$V_{KI} \bullet dC_{KI}/dt = Q_{KI} \bullet C_{ab} - Q_{KI} \bullet C_{vKI} - CL_{R,u} \bullet C_{vKI,u} \quad \text{(Eq. 3)}$$

Table I. Summary of the available preclinical pharmacokinetic data for the 19 compounds studied (all data held on file at Roche)

Compound ID	Species	CL (mL/min/kg)	V_{ss} (L/kg)	$t_{1/2}$ (h)	F (%)	CL_R (%)	k_a (h^{-1})
CPD1	Rat	13	0.87	0.93	31	0	NA
	Dog	2.3	0.79	4.5	76	0	3.1
	Pig	6.9	0.82	1.8	47	0	0.65
	Monkey	0.85	0.24	4.3	58	0	0.89
CPD2	Rat	4.5	10	26	58	0	2.0
	Dog	20	21	41	33	0	4.5
	Monkey	18	15	27	NA	0	NA
CPD3	Rat	6.0	12	23	69	0	0.66
	Dog	3.7	10	42	48	0	NA
	Monkey	19	11	12	51	0	NA
CPD4	Rat	28	0.42	0.30	197	0	NA
	Dog	26	1.2	0.90	217	0	2.3
	Monkey	15	0.66	2.1	64	0	4.0
CPD5	Rat	89	7.5	1.4	<2.0	0	2.2
	Dog	45	11	3.4	15	0	NA
	Monkey	30	9.5	4.5	6.0	0	1.6
CPD6	Rat	6.9	1.0	1.9	65	0	0.89
	Dog	4.0	1.1	6.0	82	0	NA
	Monkey	1.6	0.44	7.8	68	0	NA
CPD7	Rat	0.75	1.4	25	97	0	0.64
	Dog	1.4	1.5	38	32	0	NA
CPD8	Rat	68	10	2.1	62	10	1.4
	Dog	11	13	18	76	NA	1.5
	Monkey	13	3.6	3.4	34	NA	0.84
CPD9	Mouse	93	33	5.7	NA	NA	NA
	Rat	69	8.2	2.2	7.2	5.0–10	NA
	Dog	13	43	53	57	NA	NA
	Pig	12	27	33	NA	NA	NA
	Monkey	20	32	38	11	NA	0.69
CPD10	Mouse	90	56	7.2	18	NA	NA
	Rat	47	48	12	24	35	NA
	Dog	14	27	23	74	30	3.3
	Pig	17	42	29	NA	NA	NA
	Monkey	17	26	17	34	NA	NA
CPD11	Mouse	50	2.5	0.66	NA	0	NA
	Rat	30	2.1	1.2	274	0	NA
	Dog	5.4	3.7	9.4	101	0	0.67
	Monkey	9.1	1.7	3.2	67	0	NA
CPD12	Mouse	33	2.5	NA	44	0	NA
	Rat	15	4.2	NA	28	0	NA
	Dog	1.2	0.38	3.9	78	0	1.3
	Monkey	11	1.5	7.5	13	0	0.40
CPD13	Rat	44	3.6	1.1	14	50	1.2
	Dog	9.2	1.5	2.0	80	41	0.83

Continued next page

Table I. Contd

Compound ID	Species	CL (mL/min/kg)	V_{ss} (L/kg)	$t_{½}$ (h)	F (%)	CL_R (%)	k_a (h^{-1})
	Pig	12	1.8	2.4	48	N/A	0.64
	Monkey	13	3.2	3.8	69	42	0.51
CPD14	Mouse	6.9	0.72	3.5	65	0	NA
	Rat	5.8	1.1	3.4	51	0	NA
	Dog	1.2	0.37	4.6	81	0	1.7
	Pig	0.28	0.18	8.5	92	0	1.9
	Monkey	0.28	0.36	20	92	0	0.64
CPD15	Mouse	16	0.39	0.92	86	100	NA
	Rat	6.4	0.21	1.6	14	100	NA
	Dog	2.7	0.21	3.6	107	100	3.2
	Monkey	4.2	0.12	1.6	24	100	5.2
CPD16	Mouse	110	3.1	3.5	NA	0	NA
	Rat	5.3	0.75	2.8	62	0	1.1
	Rabbit	27	2.0	4.6	NA	0	NA
	Dog	11	1.1	1.9	81	0	NA
	Pig	11	2.6	4.9	NA	0	NA
	Monkey	13	1.7	8.8	57	0	3.7
CPD17	Mouse	5.3	0.50	2.4	NA	0	NA
	Rat	26	1.0	0.53	83	0	NA
	Dog	5.7	0.91	2.0	59	0	1.2
	Pig	15	1.8	6.1	17	0	0.81
CPD18	Mouse	50	2.2	0.58	98	0	NA
	Rat	21	1.4	1.1	29	0	2.1
	Dog	54	2.6	0.99	11	0	3.9
	Pig	11	8.2	16	42	0	NA
	Monkey	3.1	2.1	10	53	0	0.30
CPD19	Mouse	87	6.7	1.2	19	0	1.2
	Rat	41	2.7	1.6	25	0	6.5
	Dog	22	4.2	5.3	84	0	0.92
	Monkey	15	3.1	6.4	12	0	0.17

CL = clearance; **CL_R** = renal clearance; **F** = bioavailability; **k_a** = absorption rate constant; **NA** = not available; **$t_{½}$** = terminal elimination half-life; **V_{ss}** = volume of distribution at steady state.

where KI is kidney, $CL_{R,u}$ is unbound renal clearance (L/h).

For lung (equation 4):

$$V_{LU} \bullet dC_{LU}/dt = Q_{LU} \bullet C_{vb} - Q_{LU} \bullet C_{vLU} \quad \text{(Eq. 4)}$$

where LU is lung and vb is venous blood.

For arterial blood (equation 5):

$$V_{ab} \bullet dC_{ab}/dt = Q_{LU} \bullet C_{vLU} - Q_{LU} \bullet C_{ab} \quad \text{(Eq. 5)}$$

For venous blood (equation 6):

$$V_{vb} \bullet dC_{vb}/dt = \sum_i Q_i \bullet C_{vi} - Q_{LU} \bullet C_{vb} + K_{IV} \quad \text{(Eq. 6)}$$

where i is adipose, bone, brain, heart, kidney, liver, muscle, rest of body, skin and testes tissues, and K_{IV} is rate of intravenous infusion (mg/h).

For gut (equation 7):

$$V_{GU} \bullet dC_{GU}/dt = R_{abs} + Q_{GU} \bullet C_{ab} - Q_{GU} \bullet C_{vGU} \quad \text{(Eq. 7)}$$

where R_{abs} is rate of absorption (mg/h).

The physiological data used in the rat and human PBPK model are summarised in table IV. The drug-specific parameters required for input into the PBPK model include CL_{int} and CL_R (for elimination), K_p values (for distribution) and absorption rate (for absorption). The strategy and methods used

Table II. Summary of the available *in vitro* and physicochemical data for the 19 compounds studied (all data held on file at Roche)

Compound ID	MW	pKa	LogP	Species	f_{up}	b : p	*In vitro* CL_{int} (μL/min/mg or μL/min/10^6 cells)	Permeability (cm/s)[a]	Solubility (mg/mL)	Particle size (μ)
CPD1	487	A 7.3	5.6	Human Rat Dog Pig Monkey	0.0016 0.0016 0.0018 NA 0.0015	0.70 0.69 0.66 1[b] 0.74	88 HLM 360 RLM	4.2×10^{-4} and 0.18×10^{-4} at pH 5.5 and 7.4, respectively	0.000020, 0.000020, 0.00036, 0.0065 in aqueous buffer at pH 7, 8, 9 and 11, respectively, 0.011 and 0.012 in FeSSIF at pH 5.6 and pH 6.6, respectively	6.4
CPD2	566	B 4.1	6.5	Human Rat Dog Monkey	0.00095 0.00071 0.00089 NA	0.65 0.68 0.50 1[b]	2.0 HH 3.1 RH 5.5 DH	1.7×10^{-4}	0.001 in buffer at pH 7.4 0.038 and 0.047 in FeSSIF at pH 5.5 and pH 6.5, respectively	4.2
CPD3	579	B 6.5, >2.0	6.5	Human Rat Dog Monkey	0.0033 0.0031 0.0022 NA	0.69 0.77 0.77 1[b]	2.1 HH 1.8 RH 2.6 DH 5.3 CH	0.22×10^{-4}	1.4 in FeSSIF at pH 6.6	2.8
CPD4	338	B 8.0, 0.29	1.6	Human Rat Dog Monkey	0.16 0.03 0.17 NA	0.90 0.80 1[b] 1[b]	1.7 HH 9.0 RH 9.0 DH	3.3×10^{-4}	7.0 in aqueous buffer at pH 7.0	30
CPD5	295	B 10	3.0	Human Rat Dog Monkey	0.34 0.35 0.36 NA	1.6 1.8 1.5 1[b]	26 HH 26 RH 13 DH 21 CH	1.5×10^{-4}	59, 67, 18, 10, 6.0, 3.0 and 1.0 in aqueous buffer at pH 1.0, 3.0, 5.0, 7.0, 9.0, 11 and 13, respectively	25
CPD6	438	A 3.4	5.3	Human Rat Dog Monkey	0.0050 0.0050 0.0050 0.0050	1[b] 1[b] 1[b] 1[b]	0.18 HH 0.83 RH	4.4×10^{-4}	0.15 in aqueous buffer at pH 7	3.5
CPD7	632	B 4.2	6.6	Human Rat Dog	0.00070 0.0017 0.0029	0.60 0.66 0.61	0.75 HH 2.5 RH	0.35×10^{-4}	0.0013, 0.011, 0.051 in FaSSIF at pH 6.5, FeSSIF at pH 6.5 and high fat FeSSIF at pH 6.5, respectively	1.2
CPD8	430	B 10	3.3	Human Rat Dog Monkey	0.15 0.20 0.32 0.19	1.3 1.4 1.4 1[b]	1.1 HH 5.2 RH 0.24 DH	0.75×10^{-4}	8.96 in water at pH 4.92	1.7

Continued next page

Table II. Contd

Compound ID	MW	pKa	LogP	Species	f_{up}	b : p	*In vitro* CL_{int} (μL/min/mg or μL/min/10^6 cells)	Permeability (cm/s)[a]	Solubility (mg/mL)	Particle size (μ)
CPD9	424	B 9.4, 7.8	1.4	Human	0.89	1.5[b]	3.3 HLM	0.040×10^{-4}	3.0 in aqueous buffer at pH 7.5	Solution
				Mouse	NA	1[b]	53 RLM			
				Rat	0.85	2.2	15 DLM			
				Dog	0.89	1.5	9.8 PLM			
				Pig	NA	1[b]	53 CLM			
				Monkey	NA	1[b]				
CPD10	481	B 6.6, 8.5	2.5	Human	0.23	1[b]	3.4 HLM	0.67×10^{-4}	29, 21, 9.0, 5.9, 3.0, 1.8, 1.2, 1.1, 0.96, 0.87, 0.80, 0.80 in aqueous buffer at pH 6.4, 6.6, 7.1, 7.3, 7.7, 8.1, 8.6, 8.8, 9.0, 9.5, 9.6, 10.2, respectively	Solution
				Mouse	NA	1[b]	5.9 RLM			
				Rat	0.66	1.6	17 DLM			
				Dog	0.52	0.9	36 PLM			
				Pig	0.45	1[b]	17 CLM			
				Monkey	NA	1[b]				
CPD11	378	B 2.4	2.7	Human	0.018	0.69	NA	2.9×10^{-4}	0.0020 in FaSSIF at pH 7.4	1.0–5.0
				Mouse	NA	1[b]				
				Rat	0.030	0.86				
				Dog	0.027	0.67				
				Monkey	0.018	0.75				
CPD12	415	A 4.3	5.9	Human	0.0096	0.62	2.3 HH	0.58×10^{-4}	0.035 in aqueous buffer at pH 7.0	1.0
				Mouse	0.022	0.52	13 RLM			
				Rat	0.019	0.63	4.9 DLM			
				Dog	0.025	0.56	65 CLM			
				Monkey	0.010	0.52				
CPD13	318	B 9.3, 8.1	1.2	Human	0.67	1[b]	1.2 HLM	0.32×10^{-4}	22.5 in aqueous buffer at pH 7.0	10
				Rat	0.75	1[b]	3.0 RLM			
				Dog	NA	1[b]	1.9 DLM			
				Pig	NA	1[b]	6.8 PLM			
				Monkey	0.64	1[b]	1.7 CLM			
CPD14	451	A 2.9	5.8	Human	0.00057	1[b]	0.54 HH	0.98×10^{-4}	0.000010, 0.016, 0.75 in aqueous buffer at pH 1, 6.5 and 7.5, respectively	13
				Mouse	NA	1[b]	1.77 RH			
				Rat	0.00056	0.60				
				Dog	0.00058	1[b]				
				Pig	NA	1[b]				
				Monkey	NA	1[b]				

Continued next page

Table II. Contd

Compound ID	MW	pKa	LogP	Species	f_{up}	b : p	*In vitro* CL_{int} (μL/min/mg or μL/min/10^6 cells)	Permeability (cm/s)[a]	Solubility (mg/mL)	Particle size (μ)
CPD15	399	A 12, 4.7	2.9	Human	0.016	0.65[b]	No turnover	0.35×10^{-4}	60 in water at pH 7.0	1.0
				Mouse	0.043	0.65[b]				
				Rat	0.030	0.60				
				Dog	0.011	0.70				
				Monkey	0.034	0.65[b]				
CPD16	371	N	1.9	Human	0.13	0.68[b]	NA	8.3×10^{-4}	0.035 in water at pH 7.0	10–60
				Mouse	0.15	0.68[b]				
				Rat	0.12	0.67				
				Rabbit	0.12	0.68[b]				
				Dog	0.17	0.68[b]				
				Pig	0.14	0.68[b]				
				Monkey	0.21	0.68				
CPD17	491	N	5.3	Human	0.0023	0.62	3.0 HH	2.2×10^{-4}	0.0080 in water at pH 7.0	Solution
				Mouse	NA	0.61[b]	4.4 RH			
				Rat	0.0029	0.57	2.0 DH			
				Dog	0.0031	0.64				
				Pig	NA	0.61				
CPD18	338	B 3.0	2.8	Human	0.015	1[b]	0.99 HH	6.6×10^{-4}	0.0060 in aqueous buffer at pH 7.0	5.0
				Mouse	0.086	0.97	2.6 RH			
				Rat	0.044	0.79	1.8 DH			
				Dog	0.096	1	2.5 CH			
				Pig	0.015	1[b]				
				Monkey	0.046	0.87				
CPD19	400	A 8.2	4.4	Human	0.020	1	610 HLM	1.1×10^{-4}	0.22 in aqueous buffer at pH 7.0	56
				Mouse	0.020	1.1	1030 MLM			
				Rat	0.030	0.86	4730 RLM			
				Dog	0.010	0.71	260 DLM			
				Monkey	0.020	0.95				

a Permeability was measured using either a high throughput Parallel Artificial Membrane Permeation Assay[26] or using a caco-2 permeability assay[27] and converted to effective human permeability using a correlation based on compounds reported in the literature.

b Assumed value.

A = acid; **B** = base; **b : p** = blood plasma ratio; **CH** = cynomolgous monkey hepatocytes; **CL_{int}** = intrinsic clearance; **CLM** = cynomologus monkey liver microsomes; **DH** = dog hepatocytes; **DLM** = dog liver microsomes; **FaSSIF** = fasted state simulated intestinal fluid; **FeSSIF** = fed state simulated intestinal fluid; **f_{up}** = fraction unbound in plasma; **HH** = human hepatocytes; **HLM** = human liver microsomes; **MLM** = mouse liver microsomes; **MW** = molecular weight; **N** = neutral; **NA** = not available; **pKa** = acid dissociation constant; **PLM** = pig liver microsomes; **RH** = rat hepatocytes; **RLM** = rat liver microsomes.

Table III. Summary of the clinical data available for the 19 compounds studied (all data held on file at Roche)

Compound ID	Dose (mg)	Route of administration	CL or CL/F (mL/min/kg)	V_{ss} or V_z/F (L/kg)	$t_{1/2}$ (h)	C_{max} (ng/mL)	AUC (μg • h/L)	t_{max} (h)	Human PBPK prediction approach used
CPD1	1	IV	5.1	0.40	1.5	NA	47	NA	CL: physiological scaling of microsomal data (V_{max} and Km)
	1	PO	6.6	1.1	2.0	7.7	31	2.5	V_{ss}: observed rat $K_{p,u}$ values
	3	PO	8.1	1.1	1.7	24	102	3.2	
	10	PO	7.7	1.4	2.5	88	456	2.3	
	20	PO	5.7	1.0	2.3	216	987	2.7	
	40	PO	7.2	1.0	1.8	334	1 234	1.8	
	80	PO	8.1	1.7	3.0	614	2 821	3.2	
	160	PO	8.6	1.7	2.6	1 265	5 065	2.2	
CPD2	20	IV	6.0	13	63	NA	858	NA	CL: physiological scaling of hepatocyte data
	40	PO	44	26	8.5	45	234	3.1	V_{ss}: tissue composition equations
CPD3	10	PO	11	14	16	8.8	233	5.8	CL: physiological scaling of hepatocyte data (V_{max} and Km)
	30	PO	7.6	17	29	36	995	5.8	V_{ss}: tissue composition equations
	100	PO	4.9	23	54	168	4 795	5.0	
	300	PO	3.0	12	48	747	25 232	5.0	
	450	PO	2.6	13	60	1 134	43 676	5.8	
CPD4	10	PO	15	0.68	0.52	154	161	0.67	CL: physiological scaling of hepatocyte data
	25	PO	14	0.75	0.63	396	449	0.67	V_{ss}: tissue composition equations
	50	PO	9.5	2.2	2.6	1 097	1 175	0.71	
	100	PO	8.6	1.8	2.5	1 910	2 859	0.83	
	200	PO	7.7	1.9	2.8	4 122	7 479	0.79	
	400	PO	6.6	1.2	2.1	8 165	14 830	0.67	
CPD5	10	PO	3660	556	2.0	0.33	0.74	0.69	CL: physiological scaling of hepatocyte data (V_{max} and Km) V_{ss}: tissue composition equations
CPD6	0.03	PO	0.37	0.22	7.1	3.7	21	1.0	CL: physiological scaling of hepatocyte data
	0.1	PO	0.44	0.27	7.1	13	58	0.83	V_{ss}: tissue composition equations
	0.3	PO	0.50	0.30	6.7	27	161	1.7	
	1	PO	0.51	0.23	5.2	101	479	1.5	
	3	PO	0.44	0.23	6.3	303	1 725	2.2	
	10	PO	0.40	0.21	5.9	1 166	6 186	2.0	
	30	PO	0.38	0.19	5.8	3 620	20 615	1.6	
CPD7	10	PO	3.7	23	73	28	726	3.3	CL: physiological scaling of hepatocyte data
	20	PO	3.0	22	128	51	3 775	4.0	V_{ss}: $V_{ss,u}$ and semi-empirical method

Continued next page

Table III. Contd

Compound ID	Dose (mg)	Route of administration	CL or CL/F (mL/min/kg)	V_{ss} or V_z/F (L/kg)	$t_{1/2}$ (h)	C_{max} (ng/mL)	AUC (μg • h/L)	t_{max} (h)	Human PBPK prediction approach used
	50	PO	4.2	29	82	109	3 121	3.5	
	100	PO	6.8	42	72	144	3 966	3.7	
	200	PO	8.1	45	68	192	6 366	4.3	
CPD8	2.5	PO	12	21	20	2.1	49	2.6	CL: physiological scaling of hepatocyte data for CL_H, and GFR
	10	PO	9.5	14	17	14	291	3.7	ratio approach for CL_R
	25	PO	10	14	16	35	605	2.5	V_{ss}: observed rat $K_{p,u}$ values
	75	PO	8.5	11	15	165	2 209	1.8	
	150	PO	7.3	10	17	348	4 771	1.9	
	300	PO	5.1	7.1	16	902	14 029	1.8	
	400	PO	5.9	9.8	21	868	16 359	3.0	
CPD9	5	PO	312	494	25	0.24	5.6	3.8	CL: physiological scaling of microsomal data for CL_H, and GFR
	20	PO	171	1650	179	0.97	46	2.6	ratio approach for CL_R
	50	PO	147	2692	210	2.6	96	2.0	V_{ss}: $V_{ss,u}$ and semi-empirical method
	100	PO	100	2025	242	6.1	281	5.2	
	150	PO	91	1177	153	7.6	466	5.1	
CPD10	10	PO	16	72	67	3.9	177	5.7	CL: physiological scaling of microsomal data for CL_H, and GFR
	50	PO	8.5	78	104	22	1 496	5.7	ratio approach for CL_R
	125	PO	7.5	63	98	91	4 152	3.8	V_{ss}: observed rat $K_{p,u}$ values
	250	PO	6.5	55	99	332	9 901	4.0	
	375	PO	8.6	74	90	620	13 435	4.3	
CPD11	100	PO	5.8	5.9	12	468	4 089	1.0	No PBPK prediction performed
	200	PO	7.2	7.8	12	639	6 596	1.0	
	400	PO	5.6	6.8	14	1 157	16 891	1.0	
CPD12	0.1	PO	4.8	0.85	2.1	0.99	4.0	1.7	CL: physiological scaling of hepatocyte data
	0.5	PO	5.7	2.0	4.1	3.5	17	3.0	V_{ss}: tissue composition equations
	5	PO	5.0	6.1	14	30	222	4.2	
	25	PO	4.6	3.8	9.3	176	1 136	3.7	
	50	PO	5.8	7.5	14	309	1 802	3.5	
CPD13	2.5	PO	6.5	1.8	3.2	18	95	1.8	CL: physiological scaling of microsomal data for CL_H, and GFR
	5	PO	6.1	2.2	4.3	33	201	1.7	ratio approach for CL_R
	7.5	PO	6.5	2.7	4.8	43	276	1.8	V_{ss}: tissue composition equations
	10	PO	6.2	2.4	4.5	57	387	1.9	

Continued next page

Table III. Contd

Compound ID	Dose (mg)	Route of administration	CL or CL/F (mL/min/kg)	V_{ss} or V_z/F (L/kg)	$t_{1/2}$ (h)	C_{max} (ng/mL)	AUC (μg • h/L)	t_{max} (h)	Human PBPK prediction approach used
	20	PO	6.1	3.1	5.9	131	795	2.0	
	30	PO	6.8	5.5	9.0	168	1 078	1.8	
CPD14	10	PO	0.030	0.17	83	1 143	111 241	3.3	CL: physiological scaling of hepatocyte data
	30	PO	0.020	0.18	96	3 528	367 975	3.8	V_{ss}: tissue composition equations
	100	PO	0.020	0.16	111	12 033	1 458 270	3.7	
	200	PO	0.020	0.17	103	21 500	2 468 856	3.3	
	300	PO	0.020	0.17	109	33 800	4 059 444	4.0	
	500	PO	0.020	0.17	116	65 017	7 971 174	4.0	
CPD15	60	PO	3.1	2.0	7.8	2 622	4 968	0.75	CL: allometric scaling of CL_R (data from four species available)
	200	PO	3.7	0.54	1.7	8 315	13 187	1.3	V_{ss}: tissue composition equations
	600	PO	3.1	9.8	36	25 583	47 161	1.2	
	1 500	PO	3.0	3.5	13	68 572	129 306	0.92	
	3 000	PO	3.9	8.3	24	91 067	189 575	1.0	
	6 000	PO	3.3	4.4	14	208 149	489 965	1.3	
CPD16	100	PO	7.7	5.1	8.0	660	3 300	1.5	No PBPK prediction performed
	300	PO	7.0	5.2	6.6	1 730	10 400	1.6	
	1 000	PO	9.0	7.7	15	3 230	29 700	1.5	
	2 000	PO	9.7	10	12	4 690	52 000	1.8	
	4 000	PO	15	13	10	6 440	74 200	2.1	
CPD17	0.0050	PO	1.6	1.5	13	0.060	0.90	4.2	CL: physiological scaling of hepatocyte data
	0.020	PO	2.4	1.8	8.6	0.16	2.1	5.3	V_{ss}: tissue composition equations
	0.060	PO	2.1	1.7	9.5	0.54	7.4	4.7	
	0.180	PO	2.0	2.4	14	1.4	22	4.3	
CPD18	25	PO	202	14	1.1	23	46	0.56	CL: physiological scaling of hepatocyte data
	50	PO	189	20	2.6	91	204	0.71	V_{ss}: tissue composition equations
	150	PO	107	66	8.0	115	370	0.75	
	500	PO	235	161	14	388	1 495	0.88	
CPD19	1	PO	26	19	8.4	1.0	13	4.3	CL: physiological scaling of microsomal data V_{ss}: tissue composition equations

AUC = area under the plasma concentration-time curve; **CL** = clearance; **CL/F** = apparent oral clearance; $\mathbf{CL_H}$ = hepatic clearance; $\mathbf{CL_R}$ = renal clearance; $\mathbf{C_{max}}$ = peak plasma concentration; **GFR** = glomerular filtration rate; **IV** = intravenous; **Km** = Michaelis-Menten constant; $\mathbf{K_{p,u}}$ = tissue : plasma partition coefficient of unbound drug; **PBPK** = physiologically based pharmacokinetic; **PO** = oral; $\mathbf{t_{1/2}}$ = terminal elimination half-life; $\mathbf{t_{max}}$ = time to reach C_{max}; $\mathbf{V_{ss}}$ = volume of distribution at steady state; $\mathbf{V_{ss,u}}$ = volume of distribution of unbound drug at steady state; $\mathbf{V_{max}}$ = maximum rate; $\mathbf{V_z/F}$ = apparent volume of distribution during terminal phase after non-intravenous administration.

for estimating these parameters are described in the following sections.

Elimination

For compounds cleared by hepatic metabolism, *in vitro* CL_{int} values determined from hepatocyte or microsomal substrate depletion or kinetic assays were normalised for cell or microsomal protein concentration to obtain CL_{int} in units of µL/min/10^6 cells or µL/min/mg, and subsequently corrected for any nonspecific binding to give $CL_{int,u}$. Binding to microsomes was predicted using an equation proposed by Austin et al.[31] *In vitro* $CL_{int,u}$ was scaled to *in vivo* $CL_{int,u}$ using formal scaling procedures (equation 8), accounting for the microsomal recovery or hepatocellularity and liver weight as described by Houston.[15]

$$CL_{int,u}\ \textit{in vivo} = CL_{int,u}\ \textit{in vitro} \bullet SF \quad \text{(Eq. 8)}$$

where SF represents the milligrams of microsomal protein or million cells/g of liver multiplied by the grams of liver weight. Microsomal recovery (rat 60.1 mg/g; human 33–52.5 mg/g) and hepatocellularity (rat 109 million cells/g; human 107–120 million cells/g) scaling factors have been reported in the literature for rat[32] and human.[16,33,34] Units were converted to L/h for use in the PBPK model. Nonlinear metabolic processes were incorporated into the PBPK model when *in vitro* data were available, by replacing equation 2 with equation 9.

$$V_{LI} \bullet dC_{LI}/dt = Q_H \bullet C_{ab} + Q_{GU} \bullet C_{vGU} + Q_{SL} \bullet C_{vSL} - Q_{LI} \bullet C_{vLI} - \left(\frac{V_{max} \bullet SF}{Km_u + C_{vLI,u}}\right) \bullet C_{vLI,u} \quad \text{(Eq. 9)}$$

where V_{max} is the maximal velocity for metabolism (mg/h/mg microsomal protein or 10^6 cells) and Km_u is the unbound Michaelis-Menten constant (mg/L).

In all cases hepatocyte data were used in preference to microsomal data.

For renally cleared compounds, the prediction of CL_R assuming filtration (glomerular filtration rate [GFR] × f_{up}) was initially evaluated in the rat; however, under-predictions were obtained in all cases. Therefore, two other scaling methods were applied for renally cleared compounds: (i) the 'GFR ratio approach' if only minimal preclinical data were available; and (ii) allometry if CL_R information from four or more animal species was available. The 'GFR ratio approach' was proposed by Lin.[35] In brief, he observed that the ratio of $CL_{R,u}$ (when expressed per kilogram of bodyweight) for a range of compounds is approximately equal to the ratio of GFR between rat and human (4.8); therefore, with information on the CL_R in the rat, the human CL_R can be estimated (see equation 10).

$$CL_{R,u,human} = \frac{CL_{R,u,rat}}{\text{GFR ratio}} \quad \text{(Eq. 10)}$$

where the GFR ratio between rat and human = 4.8. Units were converted to L/h for use in the PBPK model.

The strategy applied in this evaluation for the prediction of elimination is shown in figure 1a. The prediction was always first evaluated in preclinical species using the available *in vitro* or *in vivo* data. Providing this prediction was accurate, a prediction to human was made under the same assumptions.

Distribution

V_{ss} was estimated using mechanistic tissue composition equations developed by Poulin and coworkers.[17-19] A detailed explanation of the mechanistic basis for these equations has been described previously.[17] Briefly, these equations assume that the drug distributes homogenously into the tissue and plasma by passive diffusion where two processes are accounted for: (i) nonspecific binding to lipids estimated from drug lipophilicity data (LogP and LogD); and (ii) specific reversible binding to common proteins present in plasma and tissue estimated from f_{up}. A generalised form of the equations published by Poulin and coworkers[17-19] is shown in equation 11.

$$K_p = \frac{(P_{NA/A} \bullet [V_{NLT} + 0.3 \bullet V_{PHT}])}{(P_{NA/A} \bullet [V_{NLp} + 0.3 \bullet V_{PHp}])} \bullet \frac{+ (1 \bullet [V_{WT} + 0.7 \bullet V_{PHT}])}{+ (1 \bullet [V_{Wp} + 0.7 \bullet V_{PHp}])} \bullet \frac{f_{up}}{f_{uT}} \quad \text{(Eq. 11)}$$

where V is the fractional tissue volume content of neutral lipids (NL), phospholipids (PH) and water

(W), $P_{NA/A}$ is the *n*-octanol-buffer partition coefficient of the non-ionised species (anti-logged value) for a non-adipose tissue or is the olive oil : buffer partition coefficient for both the non-ionised and ionised species at pH 7.4 (anti-logged value) for adipose tissue. The LogD in olive oil was calculated from the LogP using the Henderson-Hasselbalch equations (accounting for the pKa values) and the following relationship: LogP olive oil = 1.115 × LogP octanol − 1.35, as described by Poulin and Theil.[18]

For hydrophilic acids that are ionised at physiological pH, penetration into cells is limited. For these types of compounds, Poulin and coworkers[17-19] proposed equation 12.

$$K_p = \frac{V_{EST}}{V_{ESp}} \bullet \frac{f_{up}}{f_{uT}}$$

(Eq. 12)

where V_{ES} is the fractional volume content of extracellular space in tissue (T) and plasma (p). This equation assumes that under *in vivo* conditions the K_p values are approximately equal to the ratio of the fractional volume content of the extracellular space between tissues and blood.

The parameter values used for V_{NLT}, V_{NLp}, V_{PHT}, V_{PHp}, V_{WT}, V_{Wp}, V_{EST}, and V_{ESp} have been reported by Poulin and Theil.[18] The f_{uT} value used in equation 11 and equation 12 was estimated using equation 13.

$$f_{uT} = \frac{1}{1 + \frac{1 - f_{up}}{f_{up} / CR_{alb}}}$$

(Eq. 13)

where CR_{alb} is the concentration ratio of albumin between the tissue and plasma. This equation assumes that the number of binding sites and the affinity constant is similar in both the tissue and the plasma. For non-adipose tissues, CR_{alb} was assumed to equal 0.5, as proposed by Poulin and coworkers.[17-19] The same investigators assumed binding in the adipose tissue was negligible, i.e. $f_{uT} = 1$; however, for a number of lipophilic and highly protein-bound compounds, neglecting protein binding in adipose tissue may not be valid. It has been reported that for adipose tissue, CR_{alb} is equal to 0.15;[36] therefore, a drug that is highly bound to albumin in plasma would also bind to albumin in adipose tissue. For this reason, in this study the f_{uT} value for the adipose tissue was calculated using equation 13, assuming a CR_{alb} value equal to 0.15.

For those compounds where the tissue composition equations gave poor predictions of V_{ss} and profile shape in the rat, experimentally determined *in vivo* K_p values were used. This approach was used for compounds CPD1, CPD8 and CPD10; the corresponding rat K_p values are shown in table V. K_p values in human were estimated by assuming $K_{p,u,human}$ is equal to $K_{p,u,rat}$ ($K_{p,u} = K_p/f_{up}$). For comparison, K_p values in human were also estimated by assuming that $K_{p,human}$ is equal to $K_{p,rat}$. For tissues where elimination was suspected (liver and kidney), the experimentally determined K_p value was corrected for elimination using equation 14.

$$K_p = \frac{\text{Experimental } K_p}{1 - EX}$$

(Eq. 14)

where EX is the extraction ratio for the particular tissue (calculated by dividing tissue blood CL by tissue blood flow).

A semi-empirical approach for estimation of distribution was used if: (i) the tissue composition equations did not provide accurate estimates of tissue distribution in the rat; (ii) experimental K_p values were not available; (iii) the prediction of V_{ss} in all preclinical species was accurately predicted from the other preclinical species; and (iv) in the rat this semi-empirical approach resulted in significant improvements compared with the tissue composition method. This semi-empirical method is based on an approach originally proposed by Arundel.[37] In brief, this approach allows the partitioning of a compound into different tissues to be estimated from the observed *in vivo* V_{ss}, by assuming an empirical relationship between this parameter and the disappearance rate constant (K_T) for a particular tissue (except adipose). The K_T for a particular tissue is determined by Q_T and V_T and the corresponding K_p of the compound (i.e. $K_T = Q_T/[V_T \times K_p/b : p]$). Using ten compounds, it was observed that the product of K_T and *in vivo* V_{ss} (K_T [h^{-1}] × V_{ss} (L) = K_{Ti}

Table IV. Physiological parameter values for tissue volumes and blood flows in rat and human[a]

Tissues	Rat		Human	
	blood flow[b]	volume[c]	blood flow[b]	volume[c]
Adipose	0.0700	0.0760	0.0500	0.1196
Bone	0.1220	0.0415	0.0500	0.0856
Brain	0.0200	0.0057	0.1200	0.0200
Gut	0.1310	0.0270	0.1700	0.0171
Heart	0.0490	0.0033	0.0400	0.0047
Kidney	0.1410	0.0073	0.1900	0.0044
Liver	0.1750	0.0366	0.2500[d]	0.0257
Lung	1	0.0050	1	0.0076
Muscle	0.2780	0.4040	0.1700	0.4000
Skin	0.0580	0.1900	0.0500	0.0371
Spleen	0.0200	0.0020	0.0200[e]	0.0026
Testes[f]	0.0107	0.0100	0.0107	0.0100
Rest of body	0.0763	0.1100	0.0693	0.1885
Arterial blood		0.0272		0.0257
Venous blood		0.0544		0.0514
Plasma		0.0449		0.0424
Erythrocytes		0.0367		0.0347

a All tissue volumes (rat and human) and blood flow rates (rat) [except for testes] as a fraction of total bodyweight and cardiac output, respectively, were those used by Poulin and Theil.[5,18] Human cardiac output and all human tissue blood flow rates (except for spleen and testes) were obtained from Brown et al.[28]

b Fraction of cardiac output.

c Fraction of total body volume.

d The value reported for human liver blood flow (25% of the total cardiac output) corresponds to the summation of the portal vein flow (15% gut + 2% spleen) and the hepatic artery flow (8%).

e The human spleen blood flow rate was obtained from Yokogawa et al.[29]

f The rat testes tissue volume and blood flow rate were obtained from Blakey et al.[30] The human fractional values were assumed equal to the rat fractional values.

[L/h]) for each tissue was constant for a range of compounds in the rat. Based on this relationship, for subsequent compounds the K_T for a certain tissue can be estimated by simply dividing the K_{Ti} value for the particular tissue by the experimental V_{ss} value (expressed in L) for the compound. In turn, the K_p can be calculated. For the purposes of this study, this approach was adapted using a larger set of compounds (midazolam, mibefrafil, mofaroten, diazepam, diltiazem, oxazepam, quinidine, imipramine, propranolol, ethoxybenzamide, antipyrine, phenobarbital [phenobarbitone], nicotine, cefazolin, and glycerrytinic acid). Mean K_{Ti} values were calculated for each rat tissue (except adipose). They were also estimated for each human tissue, by assuming that $K_{p,u,rat} = K_{p,u,human}$, and by correcting for the differences in physiology between rat and human. These values are shown in table VI. For subsequent compounds, K_T values in human were estimated by dividing the K_{Ti} value for the particular tissue by the predicted V_{ss} value (expressed in L) for the compound. V_{ss} in human was predicted by assuming that the unbound V_{ss} ($V_{ss,u}$) was equal across species (when expressed per kilogram of bodyweight). Arundel[37] showed that this approach was not accurate for adipose tissue; therefore the K_T for this tissue was always calculated using the conventional approach, where the K_p was predicted using the tissue composition equations.

Finally, regardless of the K_p prediction method, V_{ss} was calculated using equation 15, as described previously.[38]

$$V_{ss} = \sum (V_T \bullet K_{pT}) + (V_E \bullet E:p) + V_p \quad \text{(Eq. 15)}$$

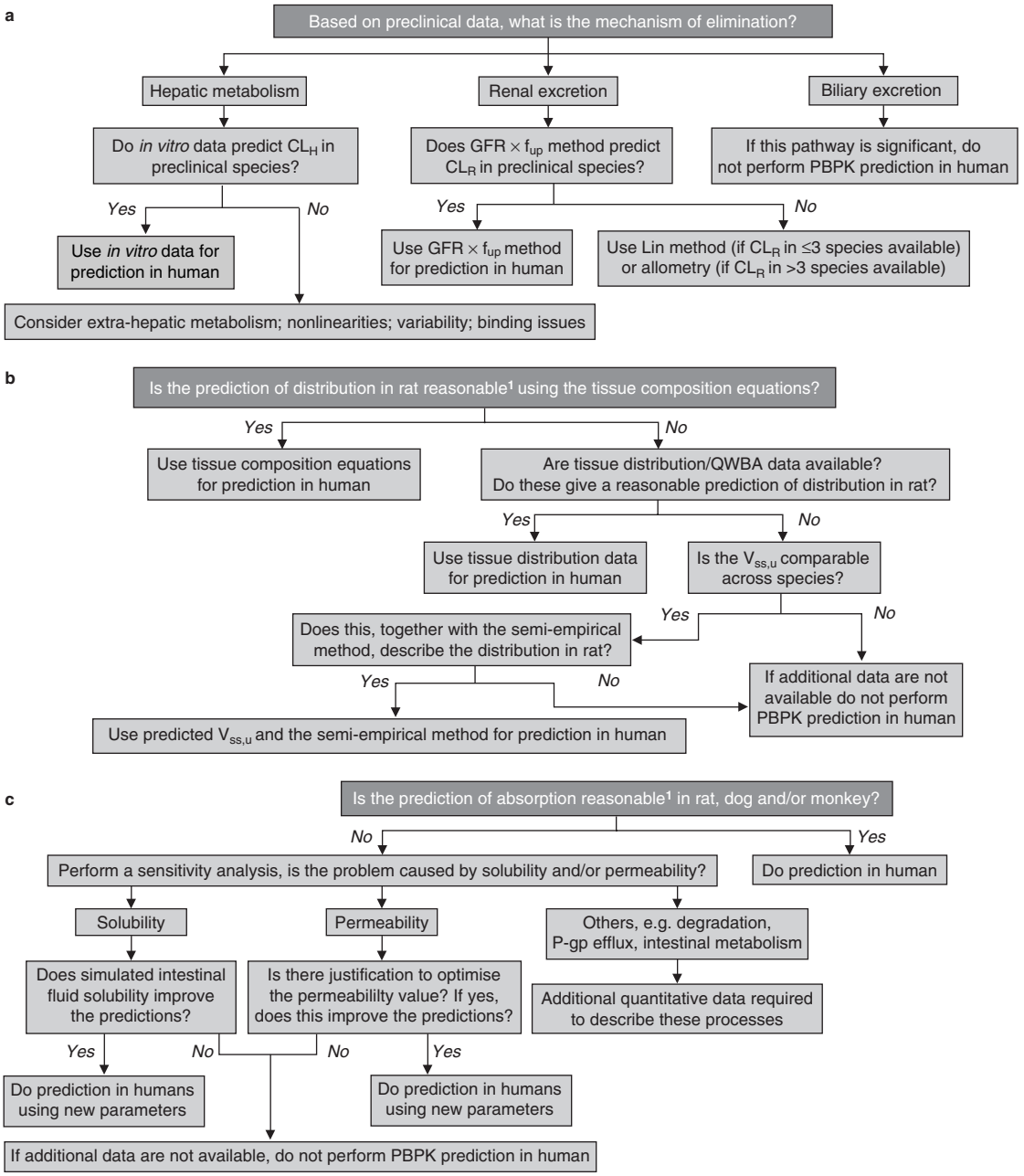

Fig. 1. Physiologically based pharmacokinetic (PBPK) prediction strategy for (**a**) elimination, (**b**) distribution and (**c**) absorption. **1** Within 3-fold error for observed and predicted parameters and plasma concentrations. **CL_H** = hepatic clearance; **CL_R** = renal clearance; **f_{up}** = fraction unbound in plasma; **GFR** = glomerular filtration rate; **P-gp** = P-glycoprotein; **QWBA** = quantitative whole body autoradiography; **$V_{ss,u}$** = volume of distribution of unbound drug at steady state.

Table V. Rat tissue : plasma partition coefficient (K_p) values for compounds CPD1, CPD8 and CPD10

Tissues	K_p value		
	CPD1	CPD8	CPD10
Adipose	0.18	2.2	7
Bone	0.18	7.8	94
Brain	0.060	0.12	2
Gut	2.4	6.5	123
Heart	0.69	5.3	15
Kidney	0.92	20	72
Liver	3.3	16	114
Lung	0.47	28	39
Muscle	0.15	10	9
Skin	0.16	14	14
Spleen	0.39	9.6	216
Testes	0.41	3.4	9

where E is erythrocyte and E : p is the erythrocyte to plasma ratio, which was estimated from b : p and the haematocrit content in blood.

The strategy applied in this evaluation for the prediction of distribution is shown in figure 1b. The prediction was first evaluated in preclinical species using the available *in vitro* or *in vivo* data. Providing this prediction was accurate, a prediction to human was made under the same assumptions.

Oral Absorption

The simulation software GastroPlus™ [1] 3.3.0 (Simulations Plus Inc., Lancaster, CA, USA) was used to predict the rate and extent of oral absorption. This was used as an input into the generic PBPK model to predict the plasma and tissue concentration-time profiles after oral administration. The model underlying GastroPlus™ is known as the Advanced Compartmental Absorption and Transit model (ACAT)[39] and is based on the original CAT model described by Yu and Amidon.[40] In brief, this ACAT model is a semi-physiologically based transit model consisting of nine compartments corresponding to different segments of the digestive tract, which describes the release, dissolution, degradation, metabolism, uptake and absorption of a compound as it transits through the different segments of the digestive tract. The simulation software uses a variety of *in vitro* and *in silico* input data such as solubility, permeability, particle size, LogP, pKa and dose, together with a series of differential equations to model the kinetics associated with each of these processes. The generic LogD model provided by Simulations Plus Inc. was used for all human absorption simulations. This LogD model adjusts absorption rate coefficients in each intestinal compartment according to pH and LogD to explain the observed rate and extent of absorption for a training set of drugs. For animal simulations the theoretical absorption model provided by Simulations Plus Inc. was used; this is based purely on physiological parameters with no optimisation.

The strategy applied in this evaluation for the prediction of absorption is shown in figure 1c. The prediction of absorption was always first evaluated in preclinical species; providing this prediction was accurate, a prediction to human was made using the same *in vitro* absorption parameters and under the same assumptions.

Summary of PBPK Prediction Strategy

The strategy for the prediction of human pharmacokinetics using PBPK modelling was as follows:

Table VI. Products (K_{Ti}) of the disappearance rate constants (K_T) and volume of distribution at steady state (V_{ss}) estimated for rat and human

Tissues	K_{Ti} (L/h)[a]	
	rat	human
Adipose	NA	NA
Bone	21	333
Brain	59	7947
Gut	27	4317
Heart	77	3442
Kidney	84	14624
Liver	19	3087
Lung	557	28646
Muscle	5.4	259
Skin	1.7	574
Spleen	59	3522
Testes	29	2285

a K_{Ti} [L/h] = K_T [h^{-1}] × V_{ss} (L).

NA = not available.

1 The use of trade names is for product identification purposes only and does not imply endorsement.

1. validation and optimisation of the disposition profile in rat;
2. validation and optimisation of the absorption profile in rat, dog and monkey;
3. intravenous and oral prediction in human.

For five compounds (CPD6, CPD13, CPD14, CPD17 and CPD18), poor predictions of elimination, distribution and/or absorption were obtained in all preclinical species. In the absence of any additional data to explain the poor simulation, a prediction to human was performed using the generic approach (hepatic metabolism for elimination, tissue composition equations for distribution and GastroPlus™ for absorption). In order to evaluate the prediction strategy reported in this study, the prediction accuracy was assessed when these compounds were both included and excluded. For two compounds (CPD11 and CPD16), no PBPK predictions could be performed as no quantitative *in vitro* metabolism data were available.

Dedrick Approach

Superposition of intravenous concentration-time profiles using Dedrick plots was performed as originally described by Dedrick et al.,[8] and more recently by Gabrielsson and Weiner.[41] Firstly, CL and V_{ss} were scaled allometrically from preclinical species as a power function of bodyweight. By default, elementary Dedrick plots were used, where pharmacokinetic time was calculated using the CL exponent (Z) as described in equation 16, and plasma concentration values were normalised for dose.

$$t_{human} = t_{animal} \bullet (BW_{human}/BW_{animal})^{1-Z} \quad \text{(Eq. 16)}$$

where BW is bodyweight.

In cases where the V_{ss} exponent (Y) determined from allometric scaling was <0.90 or >1.10, complex Dedrick plots were used, where pharmacokinetic time was calculated using both the CL and V_{ss} exponents as described in equation 17, and plasma concentration values were normalised for dose^{Y}.

$$t_{human} = t_{animal} \bullet (BW_{human}/BW_{animal})^{Y-Z} \quad \text{(Eq. 17)}$$

Pharmacokinetic time was plotted against the dose-normalised plasma concentration in each animal species. These data were analysed using a one- or two-compartmental model in WinNonlin Professional version 3.1 (Pharsight Corporation, Mountain View, CA, USA). The predicted disposition parameters were used, together with the mean absorption rate constant (k_a) and bioavailability (F) determined in animals to simulate the human oral plasma concentration-time profile using a one- or two-compartmental model with first order absorption.

Calculation of Pharmacokinetic Parameters

The observed and predicted (from the PBPK and Dedrick approaches) plasma concentration-time profiles were analysed by noncompartmental analysis using WinNonlin Professional version 3.1. Area under the plasma concentration-time curve from time zero to infinity (AUC_∞) was calculated using the trapezoidal rule, and was then extrapolated to time infinity using the apparent elimination rate constant (k_e) [determined by log-linear regression of the last three or four datapoints] and the predicted concentration at the last measurable timepoint. Peak plasma concentration (C_{max}) and time to reach C_{max} (t_{max}) were determined directly from the plasma concentration-time profiles. The apparent $t_{1/2}$ was calculated by dividing ln2 by k_e. CL (or apparent total oral clearance [CL/F]) was calculated as dose/AUC_∞. For intravenous data, V_{ss} was calculated by multiplying CL and mean residence time. Volume of distribution for the terminal phase (V_z or V_z/F) was calculated as CL (or CL/F) divided by k_e.

Assessment of Prediction Accuracy

Predicted values for CL (or CL/F), V_{ss} (or V_z/F), $t_{1/2}$, AUC, C_{max}, t_{max} and plasma concentration were assessed against the observed values using equation 18, equation 19 and equation 20. The number of doses used in the clinical study for a particular compound did not bias the prediction accuracy. An average-fold error was calculated for each compound; these values were then used to calculate an average-fold error for all compounds.

$$\text{Fold error} = \begin{cases} \dfrac{\text{predicted}}{\text{observed}}, \text{if predicted} > \text{observed} \\ \dfrac{\text{observed}}{\text{predicted}}, \text{if observed} > \text{predicted} \end{cases} \quad \text{(Eq. 18)}$$

$$\%\ \text{within x-fold error} = \%\ \text{of compounds with a fold error} \leq x \quad \text{(Eq. 19)}$$

where x = 2, 3 or 5.

$$\text{Average-fold error} = 10^{\left(\frac{1}{n}\sum(\log \text{fold error})\right)} \quad \text{(Eq. 20)}$$

This parameter uses the fold error (difference between predicted and observed *in vivo* values) for each drug, and when expressed as the geometric mean provides a measure of accuracy with equal value to under- and over-predictions.

Results

Prediction Accuracy of Plasma Concentrations

The simulated plasma concentration-time profiles for each compound, using both the PBPK and Dedrick approaches, are shown in figure 2, together with the observed data. When the simulated plasma concentrations were compared with the mean observed concentrations, the average-fold error for the PBPK and Dedrick approaches was 2.9- and 4.4-fold, respectively. In terms of the percentage of compounds with an average-fold error of less than 2-, 3- or 5-fold, PBPK was the most accurate approach, with 29%, 71% and 82% of compounds falling within those categories, respectively. When the five compounds that were judged unpredictable based on the strategy described in Methods section were excluded, the average-fold error for PBPK improved to 2.4-fold, and the percentage of compounds with an average-fold error of less than 2-, 3- or 5-fold changed to 25%, 83% and 92%, respectively.

Prediction Accuracy of Pharmacokinetic Parameters

A comparison of the observed and predicted pharmacokinetic parameters for all compounds and doses studied is shown in figure 3 and figure 4 for the PBPK and Dedrick approaches, respectively. The prediction accuracy for these parameters using the PBPK and Dedrick approaches is shown in table VII and table VIII, respectively. The prediction accuracy for each pharmacokinetic parameter is described in the following sections.

Clearance

The prediction accuracy reported in this section refers to CL when intravenous data were available, and CL/F when oral data were available. The average-fold error for the PBPK and Dedrick approaches was 2.7- and 3.4-fold, respectively. In terms of the percentage of compounds with an average-fold error of less than 2-, 3- or 5-fold, PBPK was the most accurate approach. When the five compounds that were judged unpredictable based on the strategy described in the Methods section were excluded, the average-fold error for PBPK improved to 1.7-fold, and the percentage of compounds with an average-fold error of less than 2-, 3- or 5-fold also improved (table VII).

The impact of the inclusion or exclusion of microsomal and plasma protein binding into the scaling of CL_H was investigated for CPD1 and CPD2 where clinical intravenous data were available. The incorporation of both microsomal and plasma binding values into the scaling of CL_H resulted in more accurate predictions (fold error for CPD1 and CPD2 was 1.2- and 1.4-fold, respectively) compared with those achieved when binding was ignored (fold error for CPD1 and CPD2 was 2.2- and 2-fold, respectively).

Volume of Distribution

The prediction accuracy reported in this section refers to V_{ss} when intravenous data were available and V_Z/F when oral data were available. The average-fold error for the PBPK and Dedrick approaches was 2.8- and 3.4-fold, respectively. In terms of the percentage of compounds with an average-fold error

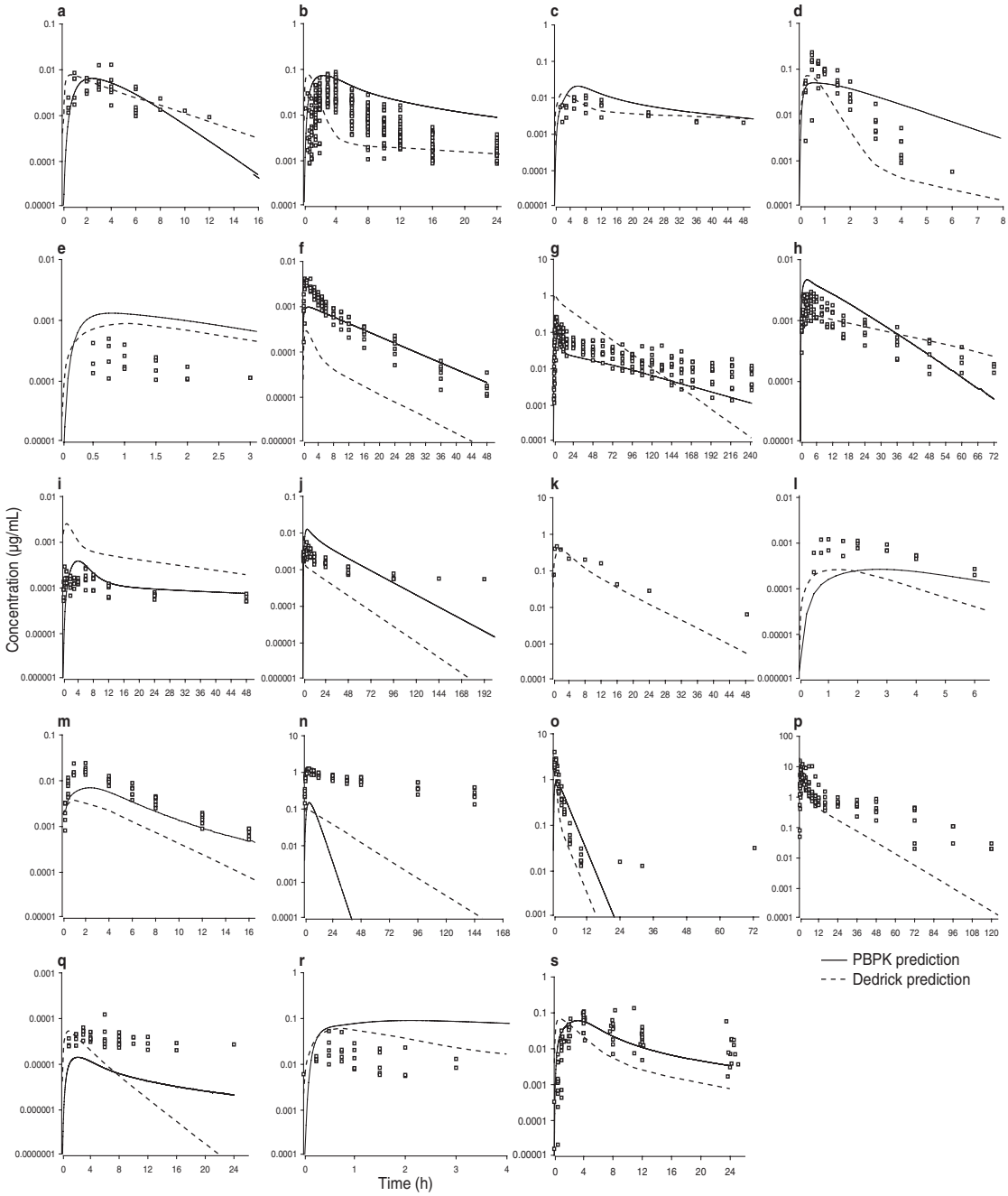

Fig. 2. Prediction of plasma concentration-time profiles using physiologically based pharmacokinetic (PBPK) and Dedrick approaches for all compounds: (**a**) CPD1; (**b**) CPD2; (**c**) CPD3; (**d**) CPD4; (**e**) CPD5; (**f**) CPD6; (**g**) CPD7; (**h**) CPD8; (**i**) CPD9; (**j**) CPD10; (**k**) CPD11; (**l**) CPD12; (**m**) CPD13; (**n**) CPD14; (**o**) CPD15; (**p**) CPD16; (**q**) CPD17; (**r**) CPD18; (**s**) CPD19. Lowest dose selected in all cases. No PBPK predictions are available for (**k**) and (**p**).

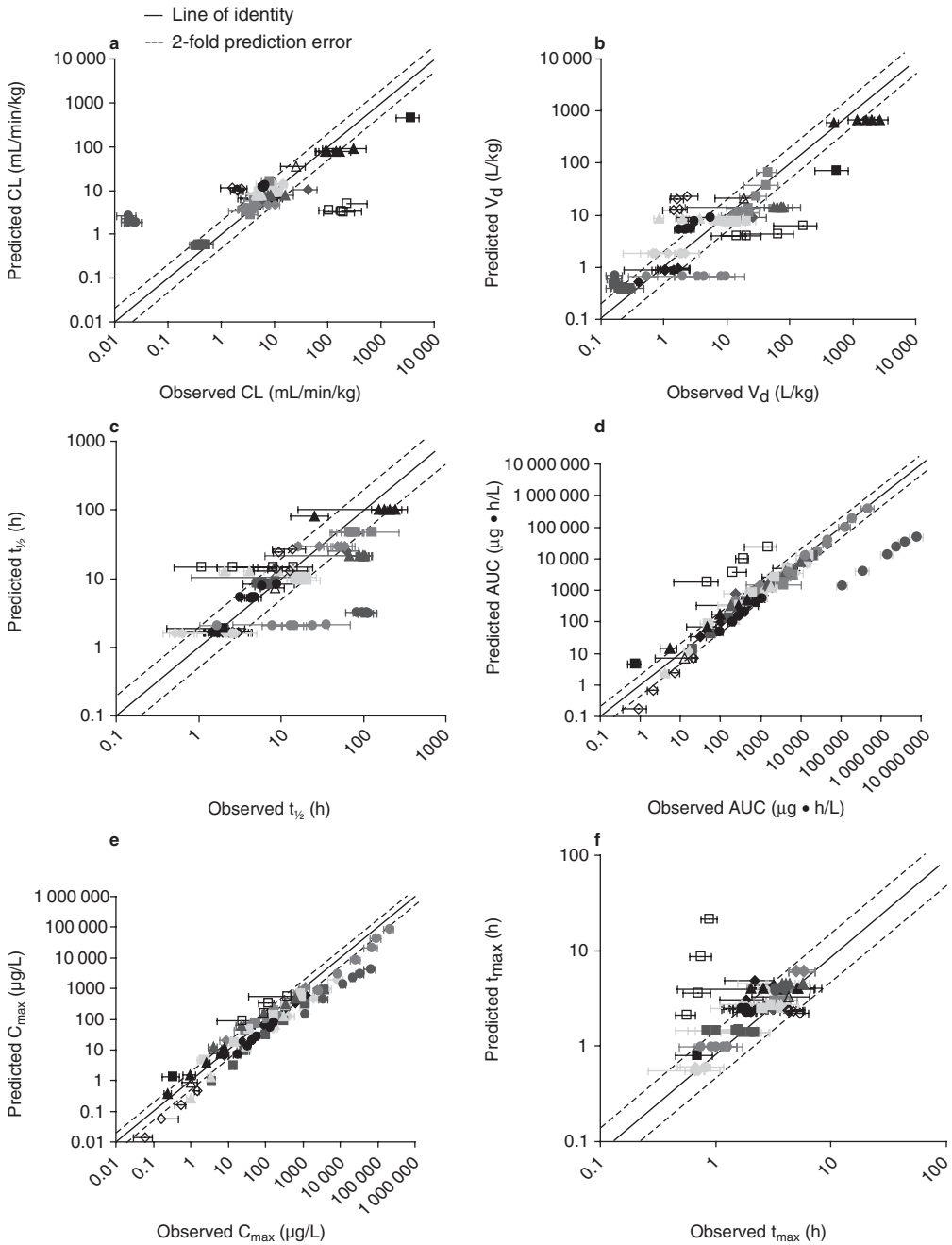

Fig. 3. Prediction accuracy for the physiologically based pharmacokinetic approach in terms of (**a**) CL, (**b**) V_d, (**c**) $t_{½}$, (**d**) AUC, (**e**) C_{max} and (**f**) t_{max}. **AUC** = area under the plasma concentration-time curve; $\mathbf{C}_{max}$ = peak plasma concentration; **CL** = clearance; $\mathbf{t}_{½}$ = terminal elimination half-life; $\mathbf{t}_{max}$ = time to reach C_{max}; $\mathbf{V}_d$ = volume of distribution.

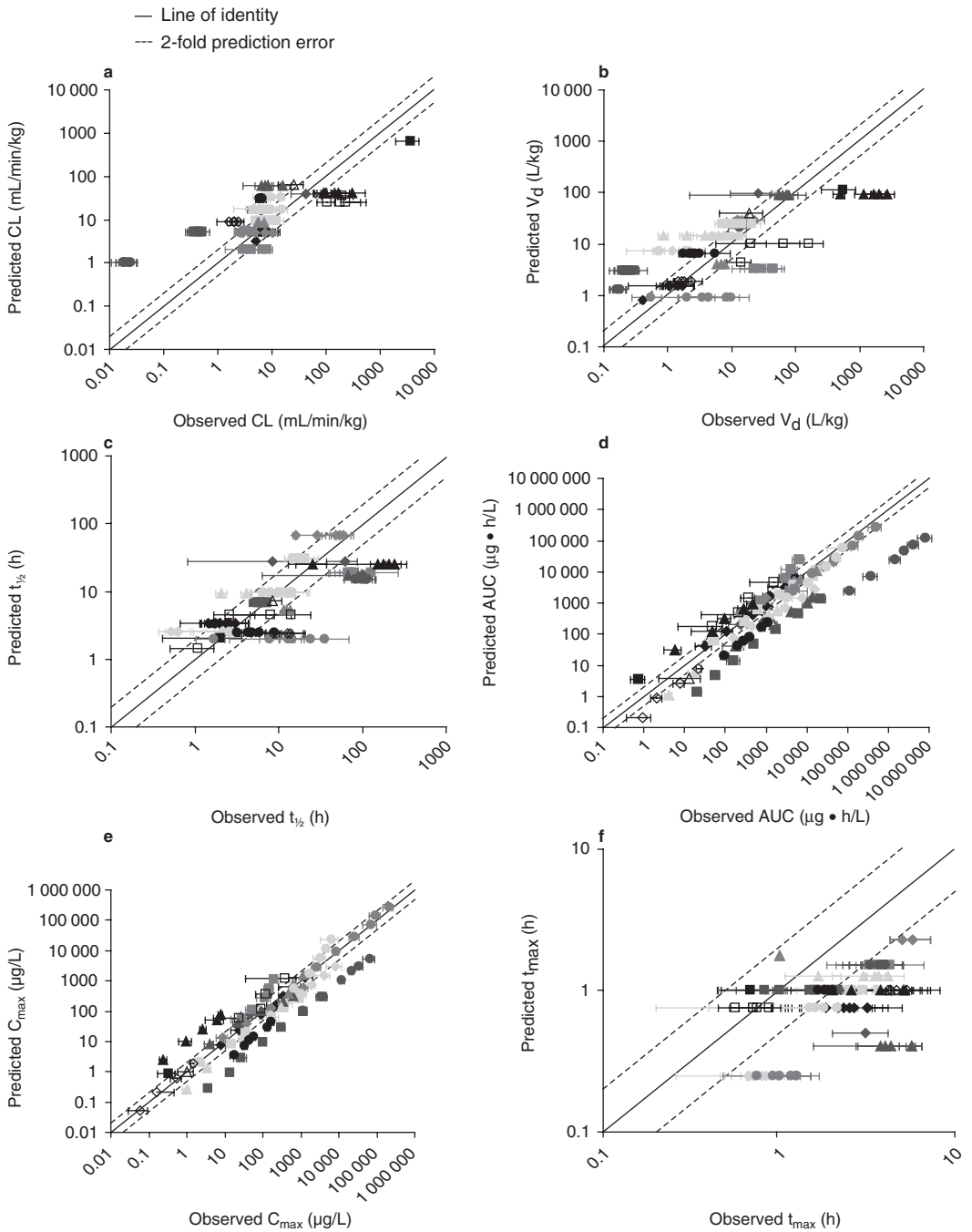

Fig. 4. Prediction accuracy for the Dedrick method in terms of (**a**) CL, (**b**) V_d, (**c**) $t_{½}$, (**d**) AUC, (**e**) C_{max} and (**f**) t_{max}. **AUC** = area under the plasma concentration-time curve; $\mathbf{C}_{max}$ = peak plasma concentration; **CL** = clearance; $\mathbf{t}_{½}$ = terminal elimination half-life; $\mathbf{t}_{max}$ = time to reach C_{max}; $\mathbf{V}_d$ = volume of distribution.

Table VII. Prediction accuracy for pharmacokinetic parameters using physiologically based pharmacokinetic (PBPK) modelling

Parameter	Average-fold error[a]	Within 2-fold error (%)[a]	Within 3-fold error (%)[a]	Within 5-fold error (%)[a]
CL or CL/F[b,c]	2.7 (1.7)	71 (83)	76 (92)	76 (92)
V_{ss} or V_z/F[b]	2.8 (2.3)	41 (50)	65 (75)	76 (83)
$t_{½}$	2.2 (1.9)	71 (75)	76 (83)	88 (92)
AUC[c]	2.6 (1.7)	76 (92)	76 (92)	82 (92)
C_{max}	2.3 (1.9)	47 (67)	71 (83)	94 (100)
t_{max}	1.4 (1.2)	94 (100)	94 (100)	94 (100)

a Values in parentheses represent prediction accuracy only for those compounds that fulfilled the criteria outlined in the strategy.

b This prediction accuracy refers to CL and V_{ss} when intravenous data were available, and CL/F and V_z/F when oral data were available.

c The slight discrepancies in prediction accuracy between AUC and CL result from the fitting of the individual observed data separately and meaning the parameters.

AUC = area under the plasma concentration-time curve; **CL** = clearance; **CL/F** = apparent oral clearance; **C_{max}** = peak plasma concentration; **$t_{½}$** = terminal elimination half-life; **t_{max}** = time to reach C_{max}; **V_{ss}** = volume of distribution at steady state; **V_z/F** = apparent volume of distribution during terminal phase after non-intravenous administration.

of less than 2-, 3- or 5-fold, PBPK was the most accurate approach. When the five compounds that were judged unpredictable based on the strategy described in the Methods section were excluded, the average-fold error for PBPK improved to 2.3-fold, and the percentage of compounds with an average-fold error of less than 2-, 3- or 5-fold also improved (table VII). The prediction accuracy of V_z/F must be treated cautiously as the selection of the observed and predicted plasma concentrations (for the terminal phase) used in its estimation are largely dependent on the investigators' choice, resulting in a high degree of subjectivity.

The semi-empirical approach used in some cases for the estimation of distribution (see Methods section) required an initial estimation of V_{ss}, which was predicted by assuming that the $V_{ss,u}$ in human is equal to the $V_{ss,u}$ in animal species. The validity of this method for estimation of V_{ss} in human was difficult to assess as limited clinical intravenous data were available; therefore, its accuracy was assessed using the rat as a predictor for dog and vice versa for all 19 compounds. The average-fold error for this method was 1.9-fold; in terms of prediction accuracy this was better than the tissue composition method (average-fold error of 3.2-fold; two compounds in human; 19 compounds in rat).

The effect of species' differences in plasma binding was also investigated by comparing two different approaches for the estimation of K_p values in

Table VIII. Prediction accuracy for pharmacokinetic parameters using the Dedrick approach

Parameter	Average-fold error[a]	Within 2-fold error (%)	Within 3-fold error (%)	Within 5-fold error (%)
CL or CL/F[b,c]	3.4	37	47	74
V_{ss} or V_z/F[b]	3.4	32	53	68
$t_{½}$	2.4	53	68	79
AUC	3.3	37	47	84
C_{max}	2.4	47	74	84
t_{max}	2.8	26	63	90

a Values in parentheses represent prediction accuracy only for those compounds that fulfilled the criteria outlined in the strategy.

b This prediction accuracy refers to CL and V_{ss} when intravenous data were available, and CL/F and V_z/F when oral data were available.

c The slight discrepancies in prediction accuracy between AUC and CL result from the fitting of the individual observed data separately and meaning the parameters.

AUC = area under the plasma concentration-time curve; **CL** = clearance; **CL/F** = apparent oral clearance; **C_{max}** = peak plasma concentration; **$t_{½}$** = terminal elimination half-life; **t_{max}** = time to reach C_{max}; **V_{ss}** = volume of distribution at steady state; **V_z/F** = apparent volume of distribution during terminal phase after non-intravenous administration.

human: (i) assuming $K_{p,human}$ is equal to $K_{p,rat}$; and (ii) assuming $K_{p,u,human}$ is equal to $K_{p,u,rat}$. These results are summarised in table IX for C_{max} and $t_{1/2}$ (no observed value for V_{ss} was available). Consideration of binding differences had no impact on the predictions for CPD1 (no species differences in f_{up}) and CPD8 (species differences in f_{up}). For CPD10 (species differences in f_{up}) the prediction of $t_{1/2}$ was better when differences in plasma binding were ignored.

Terminal Elimination Half-Life

The average-fold error for the PBPK and Dedrick approaches for $t_{1/2}$ was 2.2- and 2.4-fold, respectively. In terms of the percentage of compounds with an average-fold error of less than 2-, 3- or 5-fold, PBPK was the most accurate approach. When the five compounds that were judged unpredictable based on the strategy described in the Methods section were excluded, the average-fold error for PBPK improved to 1.9-fold, and the percentage of compounds with an average-fold error of less than 2-, 3- or 5-fold also improved (table VII). The prediction accuracy of this parameter must again be treated cautiously as the plasma concentrations used in its estimation are largely dependent on the investigators' choice, resulting in a high degree of subjectivity.

Area Under the Plasma Concentration-Time Curve

The average-fold error for the PBPK and Dedrick approaches for AUC was 2.6- and 3.3-fold, respectively. In terms of the percentage of compounds with an average-fold error of less than 2-, 3- or 5-fold, PBPK was the most accurate approach. When the five compounds that were judged unpredictable based on the strategy described in the Methods section were excluded, the average-fold error for PBPK improved to 1.7-fold, and the percentage of compounds with an average-fold error of less than 2-, 3- or 5-fold was also improved (table VII).

Table IX. Effect of tissue : plasma partition coefficient (K_p) scaling method from rat to human on peak plasma concentration (C_{max}) and terminal elimination half-life ($t_{1/2}$) prediction error

Compound ID	Parameter	Average-fold error	
		$K_{p,rat}$ = $K_{p,human}$	$K_{p,u,rat}$ = $K_{p,u,human}$
CPD1	C_{max}	1.6	1.6
	$t_{1/2}$	1.3	1.3
CPD8	C_{max}	1.5	1.4
	$t_{1/2}$	1.4	1.8
CPD10	C_{max}	1.8	1.9
	$t_{1/2}$	1.5	4.2

$K_{p,u}$ = K_p of unbound drug ($K_{p,u} = K_p/f_{up}$); f_{up} = fraction unbound in plasma.

Table X. Effect of solubility measurements on the prediction of peak plasma concentration (C_{max}) and area under the plasma concentration-time curve (AUC)

Compound ID	Parameter	Average-fold error	
		simulated intestinal media	aqueous buffer
CPD1	C_{max}	1.6	229
	AUC	1.1	980
CPD2	C_{max}	1.6	7.6
	AUC	3.2	4.2

For several low-solubility compounds, poor predictions of absorption, and subsequently AUC, were observed when solubility values obtained from aqueous media were used for oral simulations. For these compounds, solubility values measured in simulated intestinal fluid resulted in better predictions of oral plasma concentration-time profiles. This effect is demonstrated for CPD1 and CPD2 (table X). In these cases, accurate predictions of human plasma levels were achieved using simulated human intestinal fluid data, whereas under-predictions of plasma levels were observed when an aqueous solubility value was used. This effect is shown in figure 5 in terms of the oral plasma concentration-time profile. The different solubility medium also effected the prediction of C_{max}.

Figure 6 shows this trend more explicitly in the rat. In this species, the extent of absorption was under-predicted for all compounds with an aqueous buffer solubility <1 μg/mL (figure 6a). The use of data obtained from simulated intestinal fluid rather than aqueous buffer resulted in an improvement in the predictions of the oral plasma concentration-time profile and absorption (figure 6b).

The use of solubility data simulating fasted- as well as fed-state intestinal fluid was investigated for CPD7 where clinical data were available in fed and fasted conditions. Figure 7 shows how such data

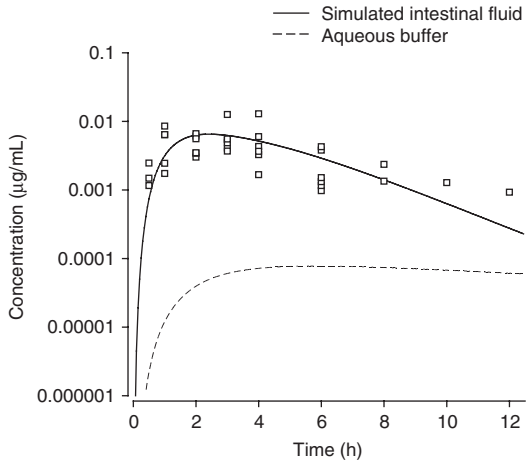

Fig. 5. Effect of different solubility media on the simulated oral plasma concentration-time profile for compound CPD1 (1mg oral administration).

were used to accurately simulate a clinical food effect.

Peak Plasma Concentration (C_{max})

The average-fold error for the PBPK and Dedrick approaches for C_{max} was 2.3- and 2.4-fold, respectively. In terms of the percentage of compounds with an average-fold error of less than 2-, 3- or 5-fold, PBPK and Dedrick approaches were similar. However, when the five compounds that were judged unpredictable based on the PBPK strategy described in the Methods section were excluded, the average-fold error for PBPK improved to 1.9-fold, and the percentage of compounds with an average-fold error of less than 2-, 3- or 5-fold also improved (table VII).

Time to Reach C_{max}

The average-fold error for the PBPK and Dedrick approaches for t_{max} was 1.4- and 2.8-fold, respectively. In terms of the percentage of compounds with an average-fold error of less than 2-, 3- or 5-fold, PBPK was the most accurate approach. When the five compounds that were judged unpredictable based on the strategy described in the Methods section were excluded, the average-fold error for PBPK improved to 1.2-fold, and the percentage of compounds with an average-fold error of less than 2-, 3- or 5-fold also improved (table VII). The prediction accuracy of this parameter must again be treated cautiously as its value is very dependent on the timepoints selected in the clinical study.

Discussion

The use of PBPK models for the extrapolation of pharmacokinetics has been limited, with only a few reports of its use in the literature.[4,42-44] However, an increasing acceptance of modelling within the pharmaceutical industry, together with a need to make more efficient and informed selection of compounds, has led to an increase in its use.[5,25,45] In contrast, allometric scaling has long been the dominant method for interspecies' scaling;[2,3,6,7] however, owing to its empirical nature and its failure to account for differences in pharmacokinetics across species, the use of this approach has come under significant criticism.[46] A PBPK strategy (with an initial validation in animals before prediction to human [see Methods section]) has been proposed and evaluated for the prediction of human pharmacokinetics. Its predictive ability was subsequently compared retrospectively with allometry (of plasma concentration-time profiles using the Dedrick approach) using 19 F. Hoffmann-La Roche compounds.

Evaluations of different extrapolation approaches have been made by other investigators;[5,47-50] however, to the best of our knowledge this represents the first piece of work where an extensive evaluation including both empirical and physiologically based methods has been made for the prediction of full plasma concentration-time profiles (intravenous and oral). It has been reported that marketed drugs, as well as being extensively characterised, tend to have different physicochemical properties to those compounds in development.[51] The dataset used for this evaluation was made up of compounds currently entering development at F. Hoffmann-La Roche and may show properties distinct from those of marketed drugs.

By following the proposed strategy for PBPK, a prediction would have been made prospectively for approximately 70% of the compounds. The proposed strategy also highlighted the importance of

initial validation in animals for a successful prediction to human. For the other 30% compounds, unacceptable prediction accuracy was obtained in animals; therefore, a prospective prediction would not have been made using PBPK. In support of this, the prediction accuracy for these compounds using PBPK was very poor. Although a number of examples in which time transformations (i.e. Dedrick approach) of preclinical data have been used to successfully predict the full plasma concentration-time profiles in humans have been published,[52-54] the prediction accuracy achieved in this study for the Dedrick approach was inferior when compared with the PBPK approach.

PBPK Approach

Assessment of Clearance

Elimination was a well predicted process using PBPK. The prediction accuracy was high for those compounds that fulfilled the criteria outlined in the strategy (83% predicted to within 2-fold error of the observed value), including an initial validation of the predictions in animals.

Compounds that were cleared mainly by hepatic metabolism were predicted accurately using PBPK. For example, CPD1, CPD3 and CPD19, three compounds where hepatic metabolism was the main elimination process, were predicted well in terms of AUC (1.1-, 1.5- and 1.9-average-fold error, respectively) and C_{max} (1.6-, 1.4- and 1.2-average-fold error, respectively). This is in agreement with exam-

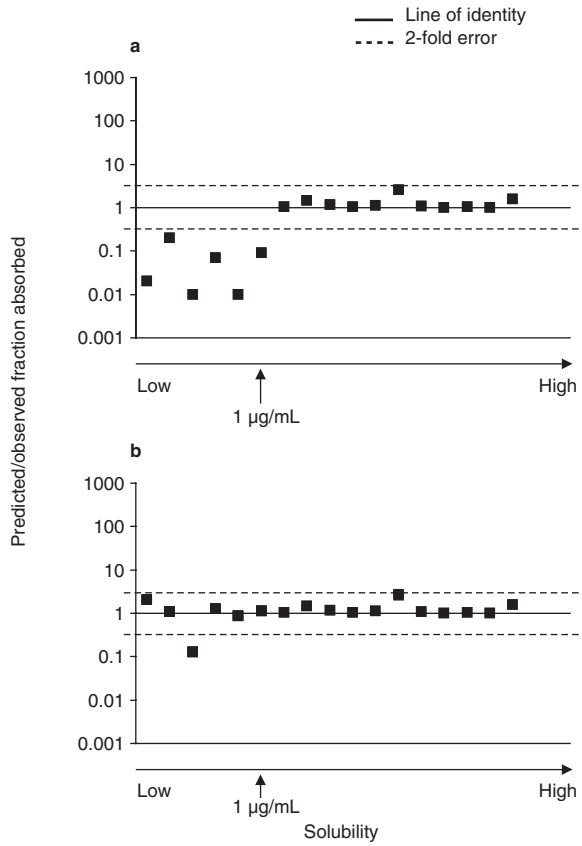

Fig. 6. Effect of different solubility media on the prediction of fraction absorbed in the rat (**a**) aqueous buffer solubility for all compounds and (**b**) simulated intestinal fluid solubility for compounds with an aqueous buffer solubility below 1 μg/mL.

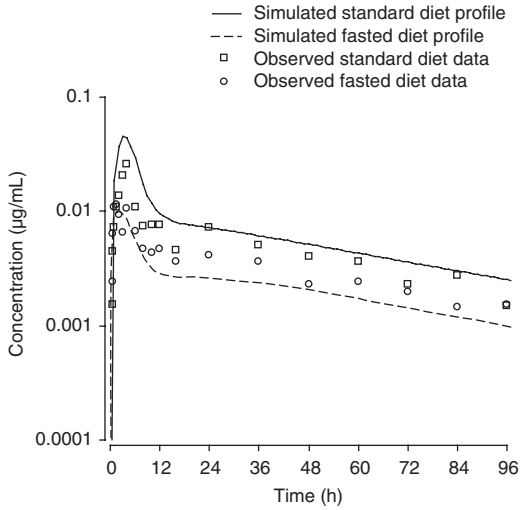

Fig. 7. Observed and predicted plasma concentration-time profiles for compound CPD7 after a standard and fasted diet.

ples in the literature where physiological approaches have been successful in predicting *in vivo* CL_H.[16,24] Predictions for renally cleared compounds were accurate using the 'GFR ratio approach'[35] and/or allometry. In support of this prediction accuracy several investigators[35,55] have achieved good predictions of CL_R using these techniques. In general, compounds that were biliary cleared were predicted poorly using the PBPK approach as this elimination pathway was ignored in all human predictions because no *in vitro* input parameters were available to describe this process. The error in AUC and C_{max} prediction was almost 100-fold and 10-fold, respectively, for CPD14, a compound cleared mainly by biliary elimination of unchanged parent. There is an established species-specific molecular weight (MW) threshold for biliary excretion (approximately 325 for rats and dogs, and approximately 500 for monkeys and humans);[56] therefore, for compounds with a MW in this range, there may be large interspecies' differences observed. Furthermore, species' differences in hepatic blood flow and bile flow do not correlate well with the biliary excretion of compounds,[57,58] thus making the scaling of this parameter across species difficult in the absence of quantitative *in vitro* information on active transport processes. Successful correlations of biliary excretion have been made in the rat between sandwich-cultured hepatocytes and *in vivo*.[59] Such techniques have not been validated with human tissue.

Intestinal metabolism represents a potential complexity for cytochrome P450 (CYP) 3A4 substrates that requires careful consideration. In this study the compounds metabolised by CYP3A4 (e.g. CPD3, CPD7 and CPD19) were predicted accurately when only hepatic metabolism was incorporated in the prediction, with no consideration of any intestinal metabolism. These results indicate that for these compounds the contribution of intestinal metabolism may be low or may only have a small impact on human pharmacokinetics; however, this is not the case for all compounds. Paine et al.[60] could only predict the CL/F of midazolam accurately by integrating human intestinal microsome data into the prediction.

Nonlinearity in metabolism represents another issue with potential impact on the accuracy of our predictions. For CPD3 and CPD5, substrate depletion data obtained from incubations performed using a range of initial substrate concentrations were fitted to the Michaelis-Menten model to estimate $Km_{apparent}$ and V_{max}. The prediction of CL for CPD3 and CPD5 was improved using this information compared with the accuracy achieved using data obtained from the typical 10 µmol/L substrate depletion incubation (data not shown).

The incorporation of both plasma and microsomal binding values into the scaling of CL_H resulted in more accurate predictions compared with those achieved when binding was ignored. This supports the unbound concentration hypothesis where the unbound concentration *in vitro* is representative of the unbound concentration in plasma, which, assuming no active uptake/efflux processes, is equal to the unbound concentration at the enzyme site. These results confirm those previously obtained by Obach,[24,61,62] where accurate predictions of CL_H were obtained when both microsomal and plasma binding were considered. Similar effects have been observed by other investigators.[21,22,31]

Assessment of Distribution

For several compounds, the tissue composition equations gave accurate predictions of distribution in both rat and human, e.g. CPD2, CPD3, CPD4, CPD5 and CPD12. However, the prediction accuracy of these equations in this study was reduced (40% within 2-fold error; two compounds in human, 19 compounds in rat) when compared with the accuracy originally observed by Poulin and Theil,[18] where from a set of 123 marketed drugs, 80% of the predictions (V_{ss} values) were within 2-fold error of the observed values.

Any discrepancies in the prediction of V_{ss} in our study might be the result of a deviation from the model assumptions of flow-limited distribution by passive diffusion. Thus, for certain compounds these equations gave poor predictions of distribution and profile shape in the rat, thus were not used for the prediction in human, e.g. CPD1, CPD7, CPD8, CPD9 and CPD10. In the rat, the observed V_{ss} values for CPD1 and CPD7 were much lower than expected based on their physicochemistry and plasma protein binding, and were not predicted accurately using the tissue composition equations. In contrast, the observed V_{ss} values for CPD8, CPD9 and CPD10 were higher than the predicted values. For CPD1 and CPD7, two very lipophilic compounds, the over-prediction of tissue distribution may have been due to a limitation in tissue diffusion (*in vitro* Caco-2 data suggested low permeability) that was not captured within the model. In support of this, a decrease in brain tissue penetration for highly lipophilic compounds has been reported in the literature.[63,64] For CPD8, CPD9 and CPD10, three strong bases, the under prediction of distribution may be explained by the failure of these equations to account for the ionic binding of strong bases to charged lipids in the tissues (i.e. acidic phospholipids such as phosphatidylserine). Yata et al.[65] demonstrated that ionic binding to phosphatidylserine was a significant process involved in the tissue distribution of three basic drugs (imipramine, propranolol and quinidine). Advancements have recently been made to incorporate such ionic binding in tissue distribution predictions.[66] In addition, the presence of active transport processes may result in over- or under-predictions of V_{ss}. For CPD6, where active transport process into the liver were observed in the rat, the tissue composition equations were not predictive, with under-predictions when extracellular distribution was assumed and over-predictions when homogenous distribution was assumed.

Based on the results obtained in this study for CPD7 and CPD9, the semi-empirical method modified from the approach originally proposed by Arundel[37] appears to give reasonable predictions; however, because of its empirical nature it should only be used when the tissue composition equations are not predictive in the rat and when rat tissue distribution data are not available. A requirement for this approach is an initial estimate of V_{ss}. In this study, this was estimated by assuming that $V_{ss,u}$ was equal across species; this assumption appeared to be valid for this compound dataset.

In cases where tissue distribution data are required for the prediction of V_{ss}, the type of tissue distribution data used must be carefully considered. For CPD1 and CPD10, quantitative whole body autoradiography data were used as steady-state tissue distribution data were unavailable and poor predictions were achieved with the tissue composition models. These compounds were moderately cleared; therefore, the majority of radioactivity measured in the experiment would have been representative of unchanged parent drug. However, for high CL compounds, caution should be taken as metabolites may represent a high proportion of the total radioactivity measured in tissues and plasma. This may have an impact on the prediction as the metabolite and parent drug will have different physicochemical properties, resulting in different tissue affinities and different distribution characteristics. In this study, the correction for differences in binding across species when scaling K_p values resulted in poorer predictions compared to when binding differences were ignored; however, the sample size was small (n = 3). Sawada et al.[38] observed that correcting K_p values for differences in plasma binding across species produced better predictions of tissue distribution than when these differences were ignored.

Assessment of Absorption

The prediction of absorption was accurate for all Biopharmaceutical Classification Scheme (BCS) Class I (high solubility and high permeability) compounds. In this dataset, there was only one BCS Class III (high solubility and low permeability) compound (CPD9) and there were no BCS Class IV (low solubility and low permeability) compounds; therefore, the limiting effect of permeability could not be assessed. For BCS Class II (low solubility and high permeability) compounds, the availability of a solubility value in simulated intestinal fluid rather than in aqueous buffer appeared imperative for an accurate prediction of the oral plasma concentration-time profiles. This was particularly evident for CPD1 and CPD2, two compounds that were poorly soluble in aqueous media. The use of an aqueous solubility value resulted in an under-prediction of plasma levels, whereas the use of solubility data measured in simulated intestinal fluid resulted in an accurate prediction of plasma levels. Such *in vitro* data offer a promising approach for the prediction of absorption for poorly soluble drugs, with the potential to also predict observed food effects, e.g. for CPD7 in this study. In support of our findings, Nicolaides et al.[67,68] demonstrated that biorelevant dissolution media could be used effectively to predict the absorption and food effects of poorly soluble lipophilic drugs.

A solubility value measured in simulated human intestinal fluid may not always be relevant for simulations in species other than human. For example, for CPD1, simulated human intestinal fluid was not appropriate for the rat. Variations in the solubility of this compound between rat and human may occur because bile salt concentrations are known to vary between species.[69] In human, bile is stored in the gall bladder; release of bile on the sight, smell or ingestion of food results in high concentrations of bile salts. In the rat, the absence of a gall bladder means that the regular release of large amounts of bile does not occur.

One way to overcome the poor predictions of *in vivo* solubility based on buffer measurements may be to correct low solubility values for bile salt concentration using an equation proposed by Mithani et al.[70] when simulated intestinal fluid data are not available. This accounts for the enhanced solubility of poorly soluble drugs as a result of the presence of bile salts in the intestinal fluids *in vivo*; however, this approach was not evaluated in this study.

Variability and Uncertainty

As is apparent from the literature[34,71] and available clinical data for the compounds studied, there is a large degree of variability in the population, both in terms of physiology (tissue volumes, blood flows, transit times, etc.) and biochemistry (plasma binding, CYP expression and activity, etc.). In order to produce predictions that are more realistic of the target population, this variability, together with any uncertainty (due to assumptions, hypotheses, handling of system, etc.), should be accounted for. The incorporation of these factors can be translated into a measure of confidence in the prediction. One important step towards this is to try to minimise uncertainty, thereby revealing the underlying variability in parameters that exist between individuals. In this context, high-quality input parameters and a thorough understanding of the pharmacokinetic processes involved are required to reduce uncertainty in the prediction. Furthermore, the following are minimum requirements with respect to input data:

- physicochemical information (LogP, LogD, pKa, MW)
- *in vitro* hepatocyte (or microsomal) metabolism data (for hepatic metabolism)
- f_{up} (for tissue distribution and hepatic metabolism)
- b : p ratio (for tissue distribution and hepatic metabolism)
- solubility measurement (for absorption)
- permeability measurement (for absorption)
- animal intravenous and oral data (for validation of models prior to human prediction)
- information on other elimination routes/uptake processes.

Nestorov et al.[72] showed that the incorporation of variability and uncertainty into the prediction of rat CL_H gave realistic predictions of the observed data. Work is currently in progress to include these factors in the form of Monte Carlo simulations.

Dedrick Approach

Allometry has been used to scale pharmacokinetic parameters and plasma concentration-time profiles as a function of bodyweight by many investigators,[2,6,7] with some success. In the literature, allometric scaling was shown to be successful for methotrexate, a renally cleared compound;[8] in contrast, unsuccessful predictions have been achieved for other renally cleared compounds.[11] In this study, AUC and C_{max} were predicted accurately for CPD15, a renally cleared compound (1.7- and 1.2-average-fold error, respectively). However, for compounds where both hepatic metabolism and renal excretion were involved, the prediction accuracy was less accurate in terms of AUC (e.g. average-fold error was 7.3- and 3-fold for CPD10 and CPD9, respectively) and C_{max} (e.g. average-fold error was 1.7- and 10-fold for CPD10 and CPD9, respectively). These poor predictions presumably are as a result of varying contributions of the different processes across species. Furthermore, predictions of CL_R may also be complicated by the different mechanisms of renal excretion across species. For some low metabolically cleared compounds the prediction accuracy in this study was good in terms of AUC (average-fold error was 1.3- and 1.6-fold for CPD1 and CPD3, respectively) and C_{max} (average-fold error was 1.1- and 1.5-fold for CPD1 and CPD3, respectively). This is surprising because for many compounds, e.g. diazepam, the enzymes responsible for its metabolism vary across species.[73]

For compounds where active transport processes were hypothesised to be involved (based on tissue distribution data and Caco-2 data), the prediction accuracy was poor in terms of AUC (13- and 55-average-fold error for CPD6 and CPD14, respectively) and C_{max} (11- and 12-average-fold error for CPD6 and CPD14, respectively). The contribution of these processes to the overall disposition of the compound may vary across species. Using PBPK, prediction accuracy was also poor. According to the PBPK strategy proposed, a prediction would not have been performed prospectively for these compounds. Lavé et al.[12] had similar poor results for napsagatran, a compound that is actively excreted into the bile and urine, with pronounced interspecies' differences in its pharmacokinetics. In agreement with reports from the literature,[8,10] poor predictions were achieved for compounds with nonlinear processes, e.g. for CPD7 (a compound with nonlinear absorption) and CPD5 (a compound with nonlinear metabolism) the prediction of AUC (average-fold error was 2.2- and 4.6-fold, respectively) and C_{max} (average-fold error was 3- and 2.6-fold, respectively) were inaccurate, and for compounds where protein binding varies across species, e.g. the prediction accuracy for CPD4 in terms of AUC and C_{max} was 3.6- and 2.6-average-fold errors, respectively.

Conclusion

The strategy for PBPK proposed in this paper led to successful predictions for approximately 70% of the compounds investigated. These successful predictions were achieved mainly for compounds that were cleared by hepatic metabolism or renal excretion, and whose absorption and distribution were governed by passive processes. Significant mis-predictions were achieved when other elimination processes (e.g. biliary elimination) or active processes were involved, or when the assumptions of flow-limited distribution and well mixed compartments were not valid. These limitations could be addressed by the addition of permeability barriers for some tissues and by the incorporation of a more complex liver model that addresses active uptake into the liver, active efflux into the bile, biliary elimination and enterohepatic recirculation; however, this will require the availability of the appropriate input data for quantification of the various processes involved as well as validation of the *in vitro* to *in vivo* scaling approaches.

A comparison of the PBPK strategy with allometry (using Dedrick plots) indicated a better accuracy for the PBPK approach; however, the potential of PBPK modelling goes beyond predicting human pharmacokinetics. PBPK modelling is a useful tool to gain insights into the properties of a compound and to understand possible reasons for poor predictions. It offers more potential in the early stages of drug discovery, in that the plasma concentration-

time profile can be predicted with the requirement of little animal *in vivo* input data. Therefore, compared with allometric methods, these methods offer a mechanism-based approach and provide the opportunity for a greater understanding of the underlying processes, ultimately resulting in a higher level of prediction accuracy.

Acknowledgements

The authors would like to thank Patrick Poulin, Alex MacDonald and Frank-Peter Theil for their assistance in this study. This work was supported by F. Hoffman La Roche. The authors have no conflicts of interest directly relevant to the content of this study.

References

1. Reigner BG, Williams PEO, Patel JH, et al. An evaluation of the integration of pharmacokinetic and pharmacodynamic principles in clinical drug development: experience within Hoffmann La Roche. Clin Pharmacokinet 1997; 33: 142-52
2. Boxenbaum H. Interspecies scaling, allometry, physiological time, and the ground plan of pharmacokinetics. J Pharmacokinet Biopharm 1982; 10: 201-27
3. Boxenbaum H. Interspecies scaling and the evolutionary comparative paradigm. Drug Metab Rev 1984; 15: 1071-121
4. Bernareggi A, Rowland M. Physiologic modelling of cyclosporine kinetics in rat and man. J Pharm Sci 1991; 19 (1): 21-50
5. Poulin P, Theil FP. Prediction of pharmacokinetics prior to in vivo studies II: generic physiologically based pharmacokinetic models of drug disposition. J Pharm Sci 2002; 91: 1358-70
6. Dedrick RL. Animal scale-up. J Pharmacokinet Biopharm 1973; 1 (5): 435-61
7. Mordenti J. Man vs beast: pharmacokinetic scaling in mammals. J Pharm Sci 1986; 75: 1028-40
8. Dedrick RL, Bischoff KB, Zaharko DS. Interspecies correlation of plasma concentration history of methotrexate (NSC-740). Cancer Chemother Rep 1970; 54: 95-101
9. Mahmood I, Balian JD. Interspecies scaling: predicting pharmacokinetic parameters of antiepileptic drugs in humans from animals with special emphasis on clearance. J Pharm Sci 1996; 85: 411-4
10. Sanwald-Ducray P, Dow J. Prediction of the pharmacokinetic parameters of reduced-dolasetron in man using in vitro-in vivo and interspecies allometric scaling. Xenobiotica 1997; 27 (2): 189-201
11. Mahmood I. Interspecies scaling of renally secreted drugs. Life Sci 1998; 63: 2365-71
12. Lavé T, Portmann R, Schenker G, et al. Interspecies pharmacokinetic comparisons and allometric scaling of napsagatran, a low molecular weight thrombin inhibitor. J Pharm Pharmacol 1999; 51: 85-91
13. Lavé T, Coassolo P, Reigner B. Prediction of hepatic metabolic clearance based on interspecies allometric scaling techniques and in vitro-in vivo correlations. Clin Pharmacokinet 1999; 36 (3): 211-31
14. Zuegge J, Schneider G, Coassolo P, et al. Prediction of hepatic metabolic clearance: comparison and assessment of prediction methods. Clin Pharmacokinet 2001; 40 (7): 553-63
15. Houston JB. Utility of in vitro drug metabolism data in predicting in vivo metabolic clearance. Biochem Pharmacol 1994; 47: 1469-79
16. Iwatsubo T, Hirota N, Ooie T, et al. Prediction of in vivo drug metabolism in the human liver from in vitro metabolism data. Pharmacol Ther 1997; 73 (2): 147-71
17. Poulin P, Theil FP. A priori prediction of tissue:plasma partition coefficients of drugs to facilitate the use of physiologically-based pharmacokinetic models in drug discovery. J Pharm Sci 2000; 89: 16-35
18. Poulin P, Theil FP. Prediction of pharmacokinetics prior to in vivo studies: I. Mechanism-based prediction of volume of distribution. J Pharm Sci 2002; 91: 129-56
19. Poulin P, Schoenlein K, Theil FP. Prediction of adipose tissue:plasma partition coefficients for structurally unrelated drugs. J Pharm Sci 2000; 90: 436-47
20. Houston JB, Carlile DJ. Prediction of hepatic clearance from microsomes, hepatocytes and liver slices. Drug Metab Rev 1997; 29: 891-922
21. Ito K, Houston JB. Comparison of the use of liver models for predicting drug clearance using in vitro kinetic data from hepatic microsomes and isolated hepatocytes. Pharm Res 2004; 21 (5): 785-92
22. Jones HM, Houston JB. Use of the substrate depletion approach for determining in vitro metabolic clearance: time dependencies in hepatocyte and microsomal incubations. Drug Metab Dispos 2004; 32 (9): 973-82
23. Lavé T, Dupin S, Schmitt C, et al. The use of human hepatocytes to select compounds based on their expected hepatic extraction ratios in humans. Pharm Res 1997; 14 (2): 152-5
24. Obach RS. Prediction of human clearance of twenty-nine drugs from hepatic microsomal intrinsic clearance data: an examination of in vitro half-life approach and nonspecific binding to microsomes. Drug Metab Dispos 1999; 27 (11): 1350-9
25. Luttringer O, Theil FP, Poulin P, et al. Physiologically based pharmacokinetic (PBPK) modelling of disposition of epiroprim in humans. J Pharm Sci 2003; 92: 1990-2007
26. Kansy M, Senner F, Gubernator K. Physicochemical high throughput screening: parallel artificial membrane permeation assay in the description of passive absorption processes. J Med Chem 1998; 41 (7): 1007-10
27. Alsenz J, Haenel E. Development of a 7-day, 96-well Caco-2 permeability assay with high-throughput direct UV compound analysis. Pharm Res 2003; 20 (12): 1961-9
28. Brown RP, Delp MD, Lindstedt SL, et al. Physiological parameter values for physiologically based pharmacokinetic models. Toxicol Ind Health 1997; 13: 407-84
29. Yokogawa K, Nakashima E, Ichimura F. Effect of fat tissue volume on the distribution kinetics of biperiden as a function of age in rats. Drug Metab Dispos 1990; 18 (2): 258-63
30. Blakey GE, Nestorov IA, Arundel PA, et al. Quantitative structure-pharmacokinetics relationships: I. Development of a whole-body physiologically based model to characterize changes in pharmacokinetics across a homologous series of barbiturates in the rat. J Pharmacokinet Biopharm 1997; 25 (3): 277-312
31. Austin RP, Barton P, Cockroft SL, et al. The influence of nonspecific microsomal binding on apparent intrinsic clearance, and its prediction from physiochemical properties. Drug Metab Dispos 2002; 30: 1497-501

32. Carlile DJ, Zomorodi K, Houston JB. Scaling factors to relate drug metabolic clearance in hepatic microsomes, isolated hepatocytes and the intact liver: studies with induced livers involving diazepam. Drug Metab Dispos 1997; 25 (8): 903-11
33. Naritomi Y, Terashita S, Kimura S, et al. Prediction of human hepatic clearance from in vivo animal experiments and in vitro metabolic studies with liver microsomes from animals and humans. Drug Metab Dispos 2001; 29 (10): 1316-24
34. Wilson ZE, Rostami-Hodjegan A, Burn JL, et al. Inter-individual variability in levels of human microsomal protein and hepatocellularity per gram of liver. Br J Clin Pharmacol 2003; 56: 433-40
35. Lin JH. Applications and limitations of interspecies scaling and in vitro extrapolation in pharmacokinetics. Drug Metab Dispos 1998; 26 (12): 1202-12
36. Ellmerer M, Schaupp L, Brunner GA, et al. Measurement of interstitial albumin in human skeletal muscle and adipose tissue by open-flow microperfusion. Am J Physiol Endocrinol Metab 2000; 278: E352-6
37. Arundel PH. A multi-compartmental model generally applicable to physiologically-based pharmacokinetics (AstraZeneca, UK) [poster]. 3rd IFAC symposium: modelling and control in biomedical systems; 1997 March 23-26; Warwick
38. Sawada Y, Hanano M, Sugiyama Y, et al. Prediction of the volume of distribution of basic drugs in human based on data from animals. J Pharmacokinet Biopharm 1984; 12: 587-96
39. Agoram B, Woltosz WS, Bolger MB. Predicting the impact of physiological and biochemical processes on oral drug bioavailability. Adv Drug Deliv Rev 2001; 50: S41-67
40. Yu LX, Amidon GL. A compartmental absorption and transit model for estimating oral drug absorption. Int J Pharm 1999; 186: 119-25
41. Gabrielsson J, Weiner D. Interspecies scaling. In: Gabrielsson J, Weiner D, editors. PK/PD data analysis: concepts and applications. Stockholm: Swedish Pharmaceutical Press, 2000: 153-174
42. Bischoff KB, Dedrick RL. Thiopental pharmacokinetics. J Pharm Sci 1968; 57: 1347-57
43. Lin JH, Sugiyama Y, Awazu S, et al. Physiological pharmacokinetics of ethoxybenzamide based on biochemical data obtained in vitro as well as on physiological data. J Pharmacokinet Biopharm 1982; 10: 649-61
44. Igari Y, Sugiyama Y, Sawada Y, et al. Prediction of diazepam disposition in the rat and man by a physiologically based pharmacokinetic model. J Pharmacokinet Biopharm 1983; 11 (6): 577-93
45. Theil FP, Haddad S, Guentert TW, et al. Utility of physiologically based pharmacokinetic models to drug development and rational drug discovery candidate selection. Toxicol Lett 2003; 138: 29-49
46. Bonate PL, Howard D. Critique of prospective allometric scaling: does the emperor have new clothes? J Clin Pharmacol 2000; 40: 335-40
47. Obach RS, Baxter JG, Liston TE, et al. The prediction of human pharmacokinetic parameters from preclinical and in vitro metabolism data. J Pharmacol Exp Ther 1997; 283: 46-58
48. Ward KW, Smith BR. A comprehensive quantitative and qualitative evaluation of extrapolation of intravenous pharmacokinetic parameters from rat, dog and monkey to humans: I. Clearance. Drug Metab Dispos 2004; 32 (6): 603-11
49. Ward KW, Smith BR. A comprehensive quantitative and qualitative evaluation of extrapolation of intravenous pharmacokinetic parameters from rat, dog and monkey to humans: II. Volume of distribution and mean residence time. Drug Metab Dispos 2004; 32 (6): 612-9
50. Brightman FA, Leahy DE, Searle GE, et al. Application of a generic physiologically-based pharmacokinetic model to the estimation of xenobiotic levels in human plasma. Drug Metab Dispos 2005; 34 (1): 94-101
51. Wenlock MC, Austin RP, Barton P, et al. A comparison of physicochemical property profiles of development and marketed oral drugs. J Med Chem 2003; 46: 1250-6
52. Lapka R, Rejholec V, Sechser T, et al. Interspecies pharmacokinetic scaling of metazosin, a novel alpha-adrenergic antagonist. Biopharm Drug Dispos 1989; 10 (6): 581-9
53. Lavé T, Saner A, Coassolo P, et al. Animal pharmacokinetics and interspecies scaling from animals to man of lamifiban, a new platelet aggregation inhibitor. J Pharm Sci 1996; 48 (6): 573-7
54. Hutchaleelaha A, Chow HH, Mayersohn M. Comparative pharmacokinetics and interspecies scaling of amphotericin B in several mammalian species. J Pharm Pharmacol 1997; 49: 178-83
55. Chapell WR, Mordenti J. Extrapolation of toxicological and pharmacological data from animals to humans. In: Testa B, editor. Advances in drug research. London: Academic Press, 1991: 1-116
56. Poggesi I. Predicting human pharmacokinetics from preclinical data. Curr Opin Drug Discov Devel 2004; 7 (1): 100-11
57. Smith RL. Excretion of drugs in bile. In: Brodie BB, Gillette JR, editors. Handbook of experimental pharmacology. Concepts in biochemical pharmacology. Vol. XXVIII. Berlin: Springer-Verlag, 1971: 354-389
58. Smith RL, editor. The excretory function of bile: the elimination of drugs and toxic substances in bile. London: Chapman and Hall, 1973
59. Liu X, Chism JP, LeCluyse EL, et al. Correlation of biliary excretion in sandwich-cultured rat hepatocytes and in vivo in rats. Drug Metab Dispos 1999; 27 (6): 637-44
60. Paine MF, Khalighi M, Fisher JM, et al. Characterization of interintestinal and intraintestinal variations in human CYP3A-dependent metabolism. J Pharmacol Exp Ther 1997; 283: 1552-62
61. Obach RS. The importance of nonspecific binding in in vitro matrices, its impact on enzyme kinetic studies of drug metabolism reactions, and implications for in vitro-in vivo correlations. Drug Metab Dispos 1996; 24 (10): 1047-9
62. Obach RS. Nonspecific binding to microsomes: impact on scale-up of in vitro intrinsic clearance to hepatic clearance as assessed through examination of warfarin, imipramine, and propranolol. Drug Metab Dispos 1997; 25 (12): 1359-69
63. Raub TJ, Barsuhn CL, Williams LR, et al. Use of a biophysical-kinetic model to understand the roles of protein binding and membrane partitioning on passive diffusion of highly lipophilic molecules across cellular barriers. J Drug Target 1993; 1 (4): 269-86
64. Sawada GA, Barsuhn CL, Lutzke BS, et al. Increased lipophilicity and subsequent cell partitioning decrease passive transcellular diffusion of novel, highly lipophilic antioxidants. J Pharmacol Exp Ther 1999; 288 (3): 1317-26
65. Yata N, Toyoda T, Murakami T, et al. Phosphatidylserine as a determinant for the tissue distribution of weakly basic drugs in rats. Pharm Res 1990; 7: 1019-25
66. Rodgers T, Leahy D, Rowland M. Physiologically based pharmacokinetic modeling 1: predicting the tissue distribution

of moderate-to-strong bases. J Pharm Sci 2005; 94 (6): 1259-76
67. Nicolaides E, Galia E, Efthymiopoulos C, et al. Forecasting the in vivo performance of four low solubility drugs from their in vitro dissolution data. Pharm Res 1998; 16 (12): 1876-82
68. Nicolaides E, Symillides M, Dressman JB, et al. Biorelevant dissolution testing to predict the plasma profile of lipophilic drugs after oral administration. Pharm Res 2001; 18 (3): 380-8
69. de Zwart LL, Rompelberg CJM, Sips AJAM, et al. Anatomical and physiological differences between various species used in studies on the pharmacokinetics and toxicology of xenobiotics: a review of the literature. Bilthoven: Research for Man and Enviroment, National Institute of Public Health and the Environment; 1999 Oct. RIVM report no. 623860 010
70. Mithani SD, Bakatselou V, TenHoor CN, et al. Estimation of the increase in solubility of drugs as a function of bile salt concentration. Pharm Res 1996; 13 (1): 163-7
71. Nestorov I. Whole body pharmacokinetic models. Clin Pharmacokinet 2003; 42 (10): 883-908
72. Nestorov I, Gueorguieva I, Jones HM, et al. Incorporating measures of variability and uncertainty into the prediction of in vivo hepatic clearance from in vitro. Drug Metab Dispos 2002; 30: 276-82
73. Jones HM, Hallifax D, Houston JB. Quantitative prediction of the in vivo inhibition of diazepam metabolism by omeprazole using rat liver microsomes and hepatocytes. Drug Metab Dispos 2004; 32 (5): 572-80

Correspondence and offprints: Dr *Hannah M. Jones*, Current address: PK and PK/PD Group, Pharmacokinetics, Dynamics and Metabolism, Pfizer Global R&D, IPC 765, 500/1.372, Ramsgate Road, Sandwich, Kent CT13 9NJ, United Kingdom.
E-mail: Hannah.jones@pfizer.com